

A framework fusing multiple representations of same processes from different 2 perspectives for robust modeling of plant interaction with hydrological processes

Xu Liang¹, Liuyan Hu¹, Hector W Clavijo¹, and Jeen-Shang Lin¹

¹University of Pittsburgh

November 24, 2022

Abstract

A modeling framework is presented for hydrological modeling to more accurately describe the water, energy, and carbon cycles and their interactions with participating processes. This framework extends the modeling strategy presented in Luo et al. (2013) by simultaneously using multiple plausible expressions, derived from different perspectives, in representing the same processes, and enforcing them together with an optimality rule and a semi-empirical expression for plant CO₂ uptake. The objectives are to reduce unconstrained free variables, mitigate parameter or variable equifinality, reduce result uncertainties, and ultimately increase the model robustness and predictability. For demonstration, the least cost optimality theory from Prentice et al. (2014), after extended to include water-limited conditions, is combined with the updated semi-empirical Ball-Berry-Leuning formulation (Tuzet et al., 2003). These two expressions are combined with other multiple expressions adopted for hydrological modeling. This framework is incorporated into both VIC+ and a modified DHSVM hydrological models with each applied to two different sites. Numerical studies are performed that using three approaches which only differ in the stomatal conductance modeling, namely, one uses the extended Prentice, one the semi-empirical, and the new framework that uses both. Results show that although all three approaches give reasonable estimates of limited measured fluxes, the present modeling framework gives much more reasonable estimates in the stomatal conductance and in other major model variables, and it also results in giving a relationship between carboxylation and transpiration that is consistent with observations. This modeling framework is general and can be adopted for other fields of study.

1
2 **A framework fusing multiple representations of same processes from different**
3 **perspectives for robust modeling of plant interaction with hydrological processes**

4
5 **Liuyan Hu, Hector W. Clavijo, Jeen-Shang Lin, and Xu Liang[‡]**

6
7 Department of Civil and Environmental Engineering, University of Pittsburgh, Pittsburgh,
8 Pennsylvania, USA.

9
10 [‡]Corresponding author: Xu Liang (xuliang@pitt.edu)

11
12
13 **Key Points:**

- 14
- 15 • A framework is presented that combines equally plausible but different formulations for
16 the same processes to improve model robustness.
 - 17 • This framework is applied to enhance carbon and water exchange modeling of plants and
18 their interactions with hydrological processes.
 - 19 • Benefits of this framework in reducing model uncertainty and mitigating variable
20 equifinality are demonstrated by numerical studies.
- 21
22
23
24

25 **Abstract**

26 A modeling framework is presented for hydrological modeling to more accurately describe the
27 water, energy, and carbon cycles and their interactions with participating processes. This
28 framework extends the modeling strategy presented in Luo et al. (2013) by simultaneously using
29 multiple plausible expressions, derived from different perspectives, in representing the same
30 processes, and enforcing them together with an optimality rule and a semi-empirical expression
31 for plant CO₂ uptake. The objectives are to reduce unconstrained free variables, mitigate
32 parameter or variable equifinality, reduce result uncertainties, and ultimately increase the model
33 robustness and predictability. For demonstration, the least cost optimality theory from Prentice
34 et al. (2014), after extended to include water-limited conditions, is combined with the updated
35 semi-empirical Ball-Berry-Leuning formulation (Tuzet et al., 2003). These two expressions are
36 combined with other multiple expressions adopted for hydrological modeling. This framework is
37 incorporated into both VIC+ and a modified DHSVM hydrological models with each applied to
38 two different sites. Numerical studies are performed that using three approaches which only
39 differ in the stomatal conductance modeling, namely, one uses the extended Prentice, one the
40 semi-empirical, and the new framework that uses both. Results show that although all three
41 approaches give reasonable estimates of limited measured fluxes, the present modeling
42 framework gives much more reasonable estimates in the stomatal conductance and in other
43 major model variables, and it also results in giving a relationship between carboxylation and
44 transpiration that is consistent with observations. This modeling framework is general and can be
45 adopted for other fields of study.

46

47

48

49 **1. Introduction**

50 With the advance in our understanding of the soil-plant-atmosphere continuum, more and more
51 important processes involved have been identified and introduced into various models. Naturally,
52 efforts have been made to add these models to the land surface or hydrological modeling system
53 to more completely and accurately describe the water, energy and carbon cycles and their
54 interactions with the various processes. Many of these processes have been studied from
55 different perspectives and the resulting models have their own merits and are considered equally
56 plausible as the current understanding could not discount one against another. But as the
57 processes involved are complex and our understanding is incomplete, these different models
58 describing the same processes often give divergent results. It is clear that these models are not
59 equivalent as Feynman (1967) remarked in his talk about the character of physical law that when
60 theories are equivalent scientifically, they give exact the same consequences. How then do we
61 use or choose among models that describe the same process but are not equivalent, especially
62 when these models each works well under some circumstances and not all circumstances?
63 Feynman further commented in the same talk, “But as long as physics is incomplete, and we are
64 trying to understand the other laws then the different formulations may give clues about what
65 might happen in other circumstances.” That is to say that different plausible models contain
66 information that could be complementary to one another, and we believe that finding ways to put
67 these incomplete pieces together is one key to answer the important question of how to reconcile
68 divergent models into better insights and solutions. Additionally, another question arises because
69 continuing bringing in new processes inevitably makes a model ever more complex and loads it
70 with a large number of parameters, some of which may not be independent while some may be
71 present as free or unconstrained variables. This may very well make a model unstable,
72 inconsistent, and intractable.

73

74 We propose to address these challenges by making use of information from available
75 perspectives simultaneously. In cases there are many plausible models, the ones with least
76 overlap in model construct are selected. That is, we will incorporate simultaneously different
77 plausible formulations or models of the same processes in the form of mutual constraints. The
78 immediate consequence of doing so will lead to reduction in the number of free variables.

79 Solutions of the processes will also become more robust, and the solutions will be less uncertain
80 and more versatile. We will show how this is done.

81 This philosophy has been successfully executed by Luo et al. (2016; 2013) into VIC+ in
82 modeling the transpiration and carbon assimilation together with other hydrological processes
83 such as hydraulic redistribution and its interactions with the groundwater table movement
84 dynamics. In that work, transpiration is simultaneously considered by (1) the method of Ohm's
85 law analogy and (2) the method of Penman-Monteith equation. For the former, transpiration is
86 estimated based on the soil water potentials in the root zone, in leaves, and of plant storage; the
87 hydraulic resistance from the soil to leaves, and between plant storage and leaves. For the latter,
88 the calculation of plant transpiration is not only driven by the meteorological factors but is also
89 directly linked to the carbon assimilation through the stomatal conductance. The carbon
90 assimilation process involved in the plant transpiration also incorporates simultaneously two
91 perspectives: (1) a diffusion method, and (2) the modified Farquhar biochemical model. That is,
92 the calculation of carbon assimilation is constrained as a consequence of the interplay of the
93 stomatal and biochemical limitations simultaneously.

94 In this study, we extend this modeling strategy to model leaf stomata. Plants play a
95 pivotal role in the soil-plant-atmosphere system, in which leaf stomata is a key in balancing
96 photosynthesis and transpiration (Bauerle & Bowden, 2011). Specifically, we simultaneously
97 consider two drastic different modeling approaches: one is based on an optimality principle,
98 while the other semi-empirical. The latter is used as an additional constraint to the former in the
99 implementation. To illustrate versatility of this extended modeling strategy in improving
100 robustness of the modeling results, we further implement them separately with two hydrological
101 models that have very different modeling structures: the VIC+ land surface model (Luo et al.,
102 2016; 2013) for large scale system and a modified high resolution version of the Distributed
103 Hydrological Soil Vegetation Model (DHSVM) (Wigmosta et al., 2002; 1994) for small scale
104 system in conducting numerical studies.

105 By controlling leaf stomata, plants exchange carbon dioxide and water with the
106 atmosphere, which can regulate water loss and adapt to external CO₂ concentration by taking
107 advantage of the biochemical and hydrological processes (Berry et al., 2010). Stomatal
108 conductance – governing plant behavior to water stress condition and photosynthesis – is one of

109 the essential components affecting water and carbon exchange process of plants.

110 Current approaches in modeling stomatal conductance can be broadly classified into four
111 categories (Damour et al., 2010; Miner et al., 2017). The first uses an empirical formulation,
112 such as the Jarvis type (Jarvis, 1976), to relate the stomatal conductance in a multiplicative form
113 to contributing factors such as solar radiation, air temperature, leaf water potential, vapor
114 pressure, and CO₂ concentration. The second uses a semi-empirical formulation to connect the
115 stomatal conductance to carbon assimilation (Ball et al., 1987; Collatz et al., 1992; Leuning,
116 1990, 1995; Tuzet et al., 2003). One widely adopted approach of this category is the simple
117 semi-empirical model based on the Ball-Berry-Leuning (BBL) formulation. This model was first
118 developed by Ball et al. (1987). Leuning et al. (1998) modified it to include the soil water
119 content. Tuzet et al. (2003) further proposed a variant form, denoted as BBL-update in this
120 study, which accounts for the leaf water potential and thus connects the root-soil-atmospheric
121 water transfer together. The third category employs a mechanistic-based water stress response
122 model that combines hydraulic control and abscisic acid (ABA) (Gutschick & Simonneau, 2002;
123 Tardieu & Davies, 1993). Models related to this third category are far more complex than the
124 first two and are not widely adopted. The fourth category employs an optimality theory. Models
125 so developed not only generally involve fewer parameters, but also better represent plants'
126 natural responses to the environment (Franklin et al., 2012). The optimality theory can provide
127 certain internal correlations among different components within a complex system (Schymanski
128 et al., 2009; Westhoff et al., 2014), and thereby reduces the number of parameters need to be
129 estimated. Currently, the semi-empirical approach and the optimality approach are the most
130 widely used methods for stomatal conductance modeling.

131 We classify the current optimality approach into three main groups following Dewar et
132 al. (2018), which is slightly different from the classifications by Wang et al. (2020) or by Sabot
133 et al. (2020). These three groups are: (1) maximizing carbon gain while minimizing the total loss
134 of water over a given time period; (2) maximizing net carbon gain at every instant in time; and
135 (3) maximizing multiple benefits for photosynthesis while minimizing associated costs at the
136 same time.

137 The first group includes models applying the water use efficiency (WUE) hypothesis –
138 the long-standing plant optimality rule by Cowan and Farquhar (Cowan, 1982; Cowan &

139 Farquhar, 1977) and its variants (e.g., (Lu et al., 2016; MÄKELÄ et al., 1996). Cowan and
140 Farquhar (1977) showed that such an optimality rule leads to an optimization constraint,
141 $\lambda = \partial A_n / \partial E_{tr}$, with λ representing a key rate of how carbon assimilation, A_n , responds to
142 transpiration, E_{tr} . This λ has been investigated for many years, yet there is still no consensus on
143 how to determine it under different conditions (Buckley et al., 2017; Wolf et al., 2016). Medlyn
144 et al. (2011) followed Cowan and Farquhar optimality rule but optimized RuBP regeneration-
145 limited photosynthesis rather than Rubisco-limited photosynthesis. Their study showed that the
146 stomatal expression by Cowan and Farquhar's optimality was similar in the form to the BBL's
147 semi-empirical expression when the atmospheric CO₂ concentration at leaf surface was much
148 higher than the compensation point. Other efforts have been made to extend the Cowan and
149 Farquhar's optimality rule in determining λ or by adding additional factors (e.g., (Katul et al.,
150 2010; 2009; Manzoni et al., 2013). A new way to solve λ is presented later in this work.

151 The second group maximizes net carbon gain and includes two subgroups. One subgroup
152 applies a penalty function to plant hydraulic behavior (Anderegg et al., 2018; Eller et al., 2018;
153 Sperry et al., 2017; Wolf et al., 2016), while the other applies a penalty function to nonstomatal
154 limitation (NSL) behavior, such as the carboxylation capacity (CAP) and mesophyll conductance
155 (MES) models by Dewar et al. (2018) and the model by Hölttä et al. (2017). Mathematically,
156 these two subgroups are similar and both maximized the carbon gain function (Dewar et al.,
157 2018; Wang et al., 2020). Biologically, CAP and MES models would produce lower
158 photosynthetic rate for the same leaf transpiration rate since more reduction factor is introduced
159 into the conductance as noted in Wang et al. (2020).

160 The third group can be viewed as a step toward a more ideal optimality rule which would
161 optimize over a broader base since all sources of benefits for photosynthesis are maximized,
162 including nitrogen, light, water, while all the associated costs are minimized at the same time
163 over multiple temporal scales as pointed out by Buckley (2017). Models belong to this group
164 include those by Manzoni et al. (2013), Prentice et al. (2014) and Buckley et al. (2017). In the
165 following, Prentice et al. (2014) model, called Prentice-2014 hereafter, is adopted as
166 representative of this third group. In Prentice-2014, the optimality rule balances the tradeoff
167 between transpiration and carboxylation capacity by minimizing the summed costs of
168 transpiration and carboxylation. Prentice-2014 employs the coordination hypothesis that under

169 typical daytime conditions, when most photosynthesis takes place, its Rubisco-limited
170 photosynthetic rate is equal to electron transport-limited photosynthetic rate. This model is
171 realized by adjusting the ratio of CO₂ within the leaf to that outside the leaf. Its limitations are
172 that it ignores the role of leaf water potential and plant hydraulics in the stomatal opening
173 (Buckley et al., 2017; Dewar et al., 2018), and thus it works best under wet conditions (Prentice
174 et al., 2014).

175 Among these three main groups of optimality rules, one main difference between the
176 WUE group (first group) and the second group is that in the former multiple factors affecting the
177 reduction of transpiration are lumped together as a total water loss through the transpiration,
178 while in the latter the reduction of transpiration is attributed specifically to either the hydraulic
179 factors, such as xylem water potential and canopy xylem pressure, or to the hydraulic and NSL
180 factors together. As a result the largest differences between them occur during the dry conditions
181 (Anderegg et al., 2018). Anderegg et al. (2018) added the water stress to the WUE group but
182 with mixed results: For 7 species among the 41 studied, the results from the WUE group using
183 the original λ rate provided comparable results with observations; while for the other 34 species,
184 results of the WUE group with the rate λ being modified by soil water potential matched
185 observations better. For all of the 41 species compared, however, they showed that results from
186 the Wolf-Anderegg-Pacala model – of the first subgroup in the second group – led to better
187 results than the WUE group with higher R² values compared to the observations. Wolf et al.
188 (2016) showed that under some special conditions where a closed form for the stomatal
189 conductance can be obtained, the optimal stomatal conductance using the optimality rule for the
190 first subgroup of the second group is remarkably similar to the semi-empirical formulation of
191 BBL, while Medlyn et al. (2011) have previously demonstrated that the stomatal conductance
192 expression based on the optimality rule for the WUE group is the same as BBL's when the
193 atmospheric CO₂ concentration at leaf surface was much higher than the compensation point.
194 Dewar et al. (2018) compared models using each of the three different groups of the optimization
195 rules and showed that the Prentice-2014 model (third group) produced similar results to those by
196 the CAP and MES models (second subgroup of the second group), but results from the WUE
197 group (first group) were different from the other two groups.

198 However, Dewar et al. (2018) also showed that CAP and Prentice-2014, as well as MES
199 and WUE (Medlyn et al., 2011) at low and large atmospheric CO₂ concentration, respectively, all
200 lead to the same one-parameter relationship between the ratio related to leaf CO₂ concentration
201 and vapor pressure deficit. The key difference among these three groups of the optimality models
202 is how each model estimates this one-parameter by its own optimization rule and the atmospheric
203 CO₂ concentration range considered. It is clear that considerable similarity exists among these
204 three different groups in terms of the functional forms in their CO₂ stomatal conductance
205 expression, although each of them is derived by associating itself with a different optimality rule.
206 Comparisons of the performance of these three different optimality modeling groups can be
207 found in Dewar et al. (2018), Anderegg et al. (2018), and Wang et al. (2020). Basically, the main
208 challenges of these approaches lie in how to define the penalty function associated with stomatal
209 opening used to balance the carbon gain and loss of water for plants under drought conditions.
210 There is yet no consensus on how this is best done.

211 In this study, the semi-empirical approach and the optimality-based approach are
212 considered equally plausible for stomatal conductance modeling because one cannot claim more
213 merits over the other with our current understanding. The framework presented in this paper
214 provides a rational way for stomatal conductance modeling by simultaneously incorporating both
215 to represent the relevant processes where appropriate. There is no reason to assume that one
216 optimization rule would work for all different processes under various conditions, as there is a
217 plethora of natural processes involved and contribute to the complex behavior of plants. But
218 because optimality-based formulations overlap and, under some scenarios, are identical as
219 discussed, we thus use only one among them. Specifically, we employ Prentice-2014 for two
220 main reasons. Firstly, it has been tested with measurements from various natural conditions and
221 experimental settings, and shown to correctly predict a number of related physiological
222 characteristics, such as the global pattern of the maximum carboxylation rate, V_{cmax} , in relation
223 to light, temperature and vapor pressure deficit (Smith et al., 2019), seasonal variations of V_{cmax}
224 across diverse ecosystems (Jiang et al., 2020), elevational trends in photosynthetic traits and
225 primary production (Peng et al., 2020), the trends in the ratio of leaf-internal to ambient CO₂
226 with respect to mean growth temperature, vapor pressure deficit, atmospheric CO₂, and elevation
227 (Wang et al., 2017). Secondly, compared with other optimality-based approaches, it has fewer
228 parameters need to be estimated and its parameters are more robust.

229 It is important to emphasize that optimization approaches should be implemented with
230 consideration of boundary conditions (Buckley et al., 2017). This is to account for factors that (1)
231 plants adjust their functional behaviors based not only on the resources provided by the
232 environment and their own maximum capabilities, but also on the fact that their physical or
233 biological properties have bounds; and (2) our descriptions and understanding of the complex
234 eco-biological processes involved are incomplete and limited, and constraints are imposed in our
235 optimization search. For example, under a drought condition, not only is the availability of water
236 to plants limited, reflected by leaf water potential, but also the physical size of the minimum and
237 maximum stomatal opening may be limited as well, leading to a constrained optimal
238 photosynthesis process. Also, due to the complex processes involved in plants' responses to
239 drought, our current descriptions or representations of the drought processes are likely
240 incomplete, leading to solutions outside feasible ranges if no bounds are imposed. Therefore,
241 upper and lower bounds posed by plant physiology should be included whenever appropriate.

242 Constraints and boundary conditions play a central role in fusing different perspectives of
243 the same process (Luo et al., 2016; 2013). Constraints limit the degrees of freedom of a model
244 caused by the large number of model parameters and their interactions. Due to the complex water
245 transport and photosynthesis process, a large number of free parameters still remains despite the
246 use of an optimality theory. A potential serious consequence may emerge in that similar model
247 responses are obtained with different and even unrealistic combinations of parameters. This
248 phenomenon is referred to as equifinality of parameter sets (Beven, 2006). Equifinality is
249 especially pronounced when (1) the number of parameters involved is large and the available
250 observations that can be simultaneously used to determine the parameter values are small; and
251 (2) there are substantial errors in the data and in the model structures. Beside the presence of
252 multiple sources of errors, one essential dominant factor leading to the equifinality pitfall is the
253 lack of constraints (Sun et al., 2020). Equifinality is pronounced in ill-posed inverse problems
254 which have insufficient constraints. In this study, we extend the equifinality description to
255 variables. That is, if similar model responses are obtained with different and unrealistic
256 combinations of values of model variables, we refer to this phenomenon as equifinality of
257 variables. Introducing constraints based on plant physiology is an effective and rational way to
258 reduce the "free" model variables, and thus the degree of the model's uncertainties (Prentice et
259 al., 2015). In a broader sense the simultaneous representation of the same process using multiple

260 expressions from different perspectives is a form of imposing constraints. The idea behind this
261 strategy, as stated earlier, is that each equally or quasi-equally plausible expression describes one
262 perspective of our understanding of the whole process. Since these expressions are not equal, it
263 implies that each of the different views gives different pieces of incomplete information about
264 the process. When brought in together, as each perspective tells one another what the process
265 should be in a specific view, they thus mutually constrain one another into a coherent and more
266 complete picture. As long as all these different expressions are equally or quasi-equally plausible
267 and not excessively overlapped, then using them at the same time would more accurately
268 describe the reality and fill the gaps that other perspectives leave. This is the modeling
269 framework we present in this study. With this approach, not only can one more accurately
270 represent the plants' behaviors under different conditions, but also reduce model's uncertainties
271 due to the removal of a large number of free variables. It is important that one is not
272 inadvertently introducing more uncertainties when adding new expressions or constraints to a
273 model trying to reduce the model's free variables. Therefore, one should always balance and
274 weigh the new expressions against the existing knowledge in assessing their relevant parameters
275 and associated uncertainties, robustness and reliability so that indeed more rational constraints,
276 rather than more uncertainties, are added.

277 In this study, we simultaneously employ two formulations to represent the stomatal
278 conductance behaviors, an optimality rule of Prentice-2014 from the third group and a semi-
279 empirical expression of Tuzet et al. (2003), or BBL-update, to illustrate the philosophy of our
280 framework. We choose these two even though they have identical forms of stomatal
281 conductance, however, the slopes of their expressions are different, and that together they cover
282 the current understanding better than other combinations. For the Prentice-2014 model, we
283 further first extend it so that it is applicable to both wet and dry conditions, and also to conditions
284 when the original coordination hypothesis of Rubisco-limited photosynthetic rate being equal to
285 the electron transport-limited photosynthetic rate does not hold. We also follow Luo et al. (2013)
286 and use both the Ohm's law analogy and the Penman-Monteith method to simultaneously
287 represent the transpiration, and employ both the diffusion method and biochemical model to
288 represent the carbon assimilation at the same time.

289 We represent the plant hydraulics considering the leaf water potential dynamics and
290 multiple stomatal conductance formulations among transpiration, photosynthesis, and carbon
291 assimilation. This is different from recent developments reviewed in Wang et al. (2020) in which
292 the plant hydraulics was only associated with one optimality rule in presenting the water stress
293 factor. The simultaneous application of an optimality rule with a semi-empirical stomatal
294 conductance formulation used in this study is unique and different from the previous efforts (De
295 Kauwe et al., 2015; Heroult et al., 2013; Manzoni et al., 2013).

296 The remainder of this paper is organized as follows: Section 2 describes the methodology
297 of our modeling framework and the underlying insights. Section 3 presents the implementation
298 of the modeling framework. Section 4 presents the results and analyses of the results between our
299 modeling framework and two other approaches with two hydrological models at four locations.
300 Conclusions are provided in Section 5.

301

302 **2. Modeling Framework: Philosophy and Construct**

303 The objectives of our modeling framework are to combine current understandings in
304 advancing modeling capability and reducing model uncertainties which are achieved through the
305 following actions: First, identify processes that have different formulations but are equally or
306 quasi-equally plausible for each activity or task of the model. In the case of describing the plant
307 stomatal behavior, for example, there are three activities involved: photosynthesis, transpiration
308 and carbon assimilation. Second, simultaneously combine these different formulations for each
309 of the process identified. Third, impose boundary conditions where appropriate. Finally, solve
310 these resulting coupled expressions.

311 The ideas and procedures of the modeling framework are explained herein in terms of the
312 incorporation of the number of modeling variables related to the photosynthesis and plant
313 transpiration processes through hydrological modeling. Conventionally, this part is formulated as
314 a five-variable problem (Anderegg et al., 2018), and the five variables are typically chosen to be
315 CO₂ stomatal conductance (g_{s,co_2}), leaf water potential (ψ_l), plant transpiration (E_{tr}), leaf CO₂
316 concentration (c_l), and carbon assimilation (A_n). Corresponding to them, our conventional

317 approach uses the following five equations: one optimality equation, two equations for
 318 transpiration, and two equations for carbon assimilation. As for the current framework, we have,
 319 however, six equations since we use two equations for stomatal conductance instead of one. This
 320 enables us to solve the posed problem with six variables that better represents the three activities
 321 (i.e., photosynthesis, transpiration and carbon assimilation) of the stomatal behavior. The
 322 selection of the additional variable is discussed below. For our new approach, we first extend the
 323 Prentice-2014 optimality model.

324 2.1 The first model for CO₂ stomatal conductance -- extended Prentice-2014 optimality
 325 model

326 As Prentice-2014 was originally developed for wet conditions, it is not expected to
 327 perform well under water-limited conditions. In this study, Prentice-2014 is extended to
 328 overcome this deficiency. In addition, the coordination hypothesis made in Prentice-2014
 329 (Prentice et al., 2014; Wang et al., 2017) between Rubisco-limitation and electron transport-
 330 limitation is not required.

331 The Prentice-2014 model minimizes the total summed cost of carboxylation and
 332 transpiration as follows,

$$333 \quad \text{Min Cost} = a \cdot E'_{tr} / A'_n + b \cdot V_{cmax} / A'_n \quad (1)$$

334 where a is the unit cost transpiration parameter; b is the unit cost carboxylation parameter; E'_{tr}
 335 [$\text{mol} \cdot \text{m}^{-2} \cdot \text{s}^{-1}$] is the transpiration; A'_n [$\text{mol} \cdot \text{m}^{-2} \cdot \text{s}^{-1}$] is net carbon assimilation; and V_{cmax} [$\text{mol} \cdot \text{m}^{-2} \cdot \text{s}^{-1}$]
 336 is the maximum carboxylation rate. E'_{tr} is calculated as follows,

$$337 \quad E'_{tr} = 1.6 \cdot g'_{s,CO_2} \cdot D' \quad (2)$$

338 where g'_{s,CO_2} [$\text{mol} \cdot \text{m}^{-2} \cdot \text{s}^{-1}$] is the CO₂ stomatal conductance; and D' [$\text{Pa} \cdot \text{Pa}^{-1}$] is the normalized
 339 leaf-to-air vapor pressure deficit calculated by $D' = [e_{sat}(T_l) - e(T_a)] / p_c$, with $e_{sat}(T_l)$ being the
 340 saturated vapor pressure at the leaf temperature, T_l , and $e(T_a)$ the actual vapor pressure at the air
 341 temperature, T_a , and p_c is the surface air pressure. V_{cmax} [$\text{mol} \cdot \text{m}^{-2} \cdot \text{s}^{-1}$] depends on T_l .

342 Furthermore, in Prentice-2014, the Rubisco activity considered in its carbon assimilation,

343 through the coordination hypothesis, is related only to CO₂ concentration within the leaf (c_i)
 344 [mol·mol⁻¹], and not to leaf water potential (ψ_l) [MPa]. For the transpiration (E'_{tr}), its g'_{s,co_2} does
 345 not include leaf water potential (ψ_l) either. Thus, Eq. (1) involves only four unknowns: E'_{tr} , g'_{s,co_2} ,
 346 A'_n , and c_i , and they are obtained by solving Eqs. (1) and (2), together with Eqs. (3) and (4)
 347 below:

$$349 \quad A'_n = g'_{s,co_2} (c_a - c_i) \quad (3)$$

$$351 \quad A'_n = V_{cmax} \frac{c_i - \Gamma^*}{c_i + K} \quad (4)$$

353 where c_a is the leaf ambient mole fractions of CO₂; K is the Michaelis–Menten coefficient for
 354 Rubisco-limited photosynthesis at a pO₂ (partial pressure of oxygen) of 21 kPa.; and Γ^*
 355 [mol·mol⁻¹] is the CO₂ compensation point which also depends on T_l .

356 It is noted here that following Dewar et al. (2018), the c_a term in g'_{s,co_2} from Prentice-
 357 2014 can be replaced by c_i and gives,

$$358 \quad g'_{s,co_2} = \frac{\xi}{\sqrt{D'}} \frac{A'_n}{c_i - \Gamma^*} \quad (5)$$

359 where ξ is defined by

$$360 \quad \frac{c_i - \Gamma^*}{c_a - \Gamma^*} = \frac{\xi}{\xi + \sqrt{D'}} \quad (6)$$

362 It will become clear later that g'_{s,co_2} of Prentice-2014 (Dewar et al., 2018) which follow
 363 Eq. (5) is clearly different from that of the BBL-updated (Tuzet et al., 2003), even though their
 364 forms are the same.

366 We extended the preceding carbon assimilation to consider leaf water potential (ψ_l) and
 367 also relax the original coordination hypothesis that Rubisco-limitation be equal to electron
 368 transport-limitation by employing a modified Farquhar model (Farquhar et al., 1980; Daly et al.,
 369 2004). In addition, we include ψ_l in the g'_{s,co_2} calculation. By doing so, Eq. (1) is extended and
 370 become applicable to water-limited conditions, and that g'_{s,co_2} and A'_n are modified to account for

371 the leaf water potential (ψ_l) and other factors affecting carbon assimilation. To avoid confusion,
 372 the modified equation uses E_{tr} and A_n without prime for transpiration and carbon assimilation,
 373 respectively, and Eq. (1) becomes,

$$374 \quad \text{Min Cost} = a \cdot E_{tr}/A_n + b \cdot V_{cmax}/A_n \quad (7a)$$

375 Following Prentice-2014 by taking the derivative of cost with respect to c_i , Eq. (7a) at optimum
 376 is given by,

$$377 \quad \frac{dCost}{dc_i} = a \cdot \frac{\partial(E_{tr}/A_n)}{\partial c_i} + b \cdot \frac{\partial(V_{cmax}/A_n)}{\partial c_i} = 0 \quad (7b)$$

378 where, in this new cost equation, both E_{tr} and A_n are functions of leaf water potential (ψ_l) as
 379 stated, and ψ_l becomes the fifth unknown variable.

380 As stated, the two perspectives of transpiration are from the Penman-Monteith equation
 381 and the Ohm's law analogy, following the approach of Luo et al. (2013). They are listed below
 382 as Eqs. (8) and (9), respectively:

$$383 \quad E_{tr} = \frac{\Delta(R_n - G) + \rho_a C_p D \bar{g}_a}{\rho_w \lambda_w (\Delta + \gamma_w + \frac{\gamma_w \bar{g}_a}{LAI g_s})} \quad (8)$$

384 where E_{tr} [$\text{m} \cdot \text{s}^{-1}$] is the transpiration; Δ [$\text{Pa} \cdot \text{K}^{-1}$] is the rate of change of saturation vapor pressure
 385 with air temperature; R_n [$\text{W} \cdot \text{m}^{-2}$] is the net radiation; G [$\text{W} \cdot \text{m}^{-2}$] is the ground heat flux; ρ_a [$\text{kg} \cdot \text{m}^{-3}$]
 386 is the air density; C_p [$\text{J} \cdot \text{kg}^{-1} \cdot \text{K}^{-1}$] is the specific heat capacity of air; D [Pa] is the vapor pressure
 387 deficit and $D = e_{sat}(T_a) - e(T_a)$; \bar{g}_a [$\text{m} \cdot \text{s}^{-1}$] is the conductance of the atmospheric boundary layer to
 388 H_2O (per unit ground area); ρ_w [$\text{kg} \cdot \text{m}^{-3}$] is the water density; λ_w [$\text{J} \cdot \text{kg}^{-1}$] is latent heat of water
 389 vaporization; γ_w [$\text{Pa} \cdot \text{K}^{-1}$] is psychrometric constant; LAI is the leaf area index; and g_s [$\text{m} \cdot \text{s}^{-1}$] is
 390 the stomatal conductance to H_2O per unit leaf area. Note that the H_2O stomatal conductance
 391 expressed as $g_{s, \text{H}_2\text{O}}$ [$\text{mol} \cdot \text{m}^{-2} \cdot \text{s}^{-1}$] is the same as stomatal conductance g_s [$\text{m} \cdot \text{s}^{-1}$] but with a

392 different unit, and g_{s,H_2O} is equal to $1.6 \cdot g_{s,CO_2}$ when both take the unit of $[\text{mol} \cdot \text{m}^{-2} \cdot \text{s}^{-1}]$.

393 Equation (9) is expressed as,

$$394 \quad E_{tr} = \frac{\psi_p - \psi_l}{r} + \frac{\psi_{soil} - \psi_l}{R} \quad (9)$$

395 where ψ_p [Pa] is the water potential of plant storage; ψ_l [Pa] is the leaf water potential; ψ_{soil} [Pa]
 396 is the lumped soil water potential in the root zone; r [$\text{Pa} \cdot \text{s} \cdot \text{m}^{-1}$] is the hydraulic resistance
 397 between plant storage and leaves; R [$\text{Pa} \cdot \text{s} \cdot \text{m}^{-1}$] is the total hydraulic resistance, a function of
 398 ψ_{soil} , from the soil to the leaves. Further details about Eq. (9) can be found in Luo et al. (2013).

399 The carbon assimilation (A_n) which has appeared in Eq. (7) is hereby formulated using
 400 both the modified Farquhar model (e.g., (Daly et al., 2004; Farquhar et al., 1980) and the
 401 diffusion method which are represented by Eqs. (10) and (11), respectively, as follows,

$$402 \quad A_n = A_{\psi_l}(\psi_l) \times A_{\phi, c_i, T_l}(\phi, c_i, T_l) \quad (10)$$

$$403 \quad A_n = g_{sba, CO_2} \cdot (c_a - c_i) \quad (11)$$

404
 405 where A_n [$\text{mol} \cdot \text{m}^{-2} \cdot \text{s}^{-1}$] is carbon assimilation; and in Eq. (10), $A_{\psi_l}(\psi_l)$ is a function related to
 406 leaf water potential, reflecting the reduction of carbon assimilation under water stressed
 407 conditions. $A_{\phi, c_i, T_l}(\phi, c_i, T_l)$ is the Farquhar model of biochemical carbon assimilation under well-
 408 watered condition, and it depends on photosynthetically active radiation (ϕ), CO_2 concentration
 409 (c_i) within the leaf, and leaf temperature (T_l).

410 The term $A_{\phi, c_i, T_l}(\phi, c_i, T_l)$ is expressed by the minimum of A_c and A_q , where A_c is the
 411 assimilation rate restricted by Rubisco activity (i.e., restricted by c_i), and A_q is the assimilation
 412 rate limited by RuBP regeneration when ϕ is low. The triose phosphate utilization (TPU)
 413 limitation and the quadratically smooth transition approach used in Daly et al. (2004) to obtain
 414 the minimum A_n from Collatz et al. (1991) are not used here as the smooth approach and TPU
 415 limitation lead to underestimation of the A_n (Rogers et al., 2021). The relevant equations for

416 these parameters are:

$$417 \quad A_{\psi_l}(\psi_l) = \begin{cases} 0 & (\psi_l < \psi_{lA0}) \\ \frac{\psi_l - \psi_{lA0}}{\psi_{lAI} - \psi_{lA0}} & (\psi_{lA0} < \psi_l < \psi_{lAI}) \\ 1 & (\psi_l > \psi_{lAI}) \end{cases} \quad (12)$$

418 where ψ_l [Pa] is the leaf water potential; ψ_{lAI} [Pa] is the leaf water potential value in well-watered
419 condition; ψ_{lA0} [Pa] is the leaf water potential value below which assimilation is reduced to zero.

$$420 \quad A_c = V_{cmax} \frac{c_i - \Gamma^*}{c_i + K_c(1 + o_i/K_o)} \quad (13)$$

421 where o_i [mol·mol⁻¹] is the oxygen concentration; K_c and K_o are the Michaelis-Menten
422 coefficients for CO₂ and O₂, respectively, which depends on T_l .

$$423 \quad A_q = \frac{J \cdot (c_i - \Gamma^*)}{4(c_i + 2\Gamma^*)} \quad (14)$$

424 where J [mol·m⁻²·s⁻¹] is the electron transport rate which depends on ϕ and T_l .

425 As for the diffusion method of Eq. (11), g_{sba,co_2} in Eq. (11) is represented by

$$426 \quad g_{sba,co_2}(\psi_l) = \left(g_{s,co_2}^{-1}(\psi_l) + g_{a,co_2}^{-1} + g_{b,co_2}^{-1} \right)^{-1} \quad (15)$$

427 where g_{a,co_2} [mol·m⁻²·s⁻¹] is the atmospheric conductance, and g_{b,co_2} [mol·m⁻²·s⁻¹] is the CO₂ leaf
428 boundary layer conductance. We note that $g_{s,co_2}(\psi_l)$ is related to leaf water potential, while
429 g'_{s,co_2} in Eqs. (2) and (3) is not since g'_{s,co_2} is only for not water-limited condition.

430 This extended least cost optimality of Prentice-2014, denoted as *LC-extended* (for
431 extended Least Cost) hereafter, is extended to water-limited conditions and to the situations
432 where the coordination hypothesis on having $A_n = A_c = A_q$ is relaxed, allows the five unknowns of
433 E_{tr} , g_{s,co_2} , A_n , c_i , and ψ_l to be obtained by solving Eqs. (7)-(11) together. *LC-extended* as
434 presented is shown works under both wet and water-limited conditions in the numerical study

435 section.

436 2.2 The second model for CO₂ stomatal conductance – BBL-updated formulation

437 Our second perspective uses BBL-updated and we make use of the fact that g_{s,co_2} is
 438 explicitly related to the CO₂ assimilation A_n , c_i , and the empirical function of $f(\psi_l)$. This BBL-
 439 updated relationship is expressed as follows,

$$440 \quad g_{s,co_2} = g_0 + \frac{a' A_n}{c_i - \Gamma^*} f(\psi_l) \quad (16)$$

441 where g_0 [$\text{mol}\cdot\text{m}^{-2}\cdot\text{s}^{-1}$] is the stomatal conductance at the light compensation point; a' is an
 442 empirical slope coefficient which varies between $[0, a'_{max}]$ where a'_{max} is the upper bound of a' ,
 443 Γ^* [$\text{mol}\cdot\text{mol}^{-1}$] is the CO₂ compensation point; and $f(\psi_l)$ is an empirical function of stomatal
 444 sensitivity to leaf water potential which varies between $[0, 1]$. Eq. (16) is widely used and
 445 validated with observations for obtaining plant CO₂ stomatal conductance.

446 Eq. (16) has a slope of $a'f(\psi_l)$ which is different from the slope of $\frac{\xi}{\sqrt{D'}}$ given by Eq. (5).

447 The slope $a'f(\psi_l)$ varies between $[0, a'_{max}]$, while the slope of $\frac{\xi}{\sqrt{D'}}$ ranges between $[0, +\infty)$ in
 448 principle as D' might approach zero. This is what we mean that the *Semi-empirical* approach,
 449 i.e., BBL-updated, is different from the Prentice-2014, and for that matter, different from the
 450 extended Prentice et al. (2014). To implement our philosophy of combining different
 451 perspectives in our new approach, *LC-extended* and Eq. (16) of BBL-update are simultaneously
 452 considered.

453 That is, by adding Eq. (16), the problem now has six equations. For that, we also choose
 454 a' as the sixth variable. Does the choice of a' as a new unknown make sense? Value of a' has
 455 been assumed a constant for a given vegetation type and is predetermined via model calibration
 456 in practice. But Miner et al. (2017) have showed that a' changes under elevated CO₂ and water
 457 stressed conditions, thus, its selection here as an unknown time-varying variable incorporates
 458 their findings.

459 It can be shown that a' has an upper limit, a'_{max} , that is vegetation type dependent related

460 to the slope in the original BBL model. This slope can be obtained using field measurements.
 461 Miner et al. (2017) provided a summary table for the slope values of the original BBL model for
 462 different plant species. Thus, the maximum slope value of a' (i.e., a'_{max}) in Eq. (16) can be
 463 derived through the relationship between the original BBL model and the BBL-updated model.
 464 In this way, a' varies over time according to the changes in water stress and CO₂ concentration
 465 level. Such a treatment on a' is more consistent with the observations by Miner et al. (2017) as
 466 stated.

467 When comparing Eq. (16) with the model of Medlyn et al., (2011), one can obtain the
 468 relationship between a' and g_l below,

$$469 \quad g_l = \left(\frac{a' c_a}{c_i - \Gamma^*} f(\psi_l) - 1 \right) \cdot \sqrt{D' * p_c} \quad (17)$$

470 where g_l is the slope value in Medlyn et al. (2011) and can be computed from a' .

471 From g_l , one can easily obtain the values of λ . With Eq. (17), g_l or λ associated with the
 472 WUE approach can be estimated at each time step via a' . With this, we may have indirectly
 473 addressed the longstanding problem to some extent of how to represent the varying nature of λ at
 474 all time scales based on the WUE optimality rule as demonstrated later.

475

476 **3. Numerical Studies**

477 To investigate the effectiveness and implications of the present framework, a series of
 478 numerical studies are conducted with two hydrological models. Two hydrological models are
 479 used simply to show that the framework works in different hydrological scales. The numerical
 480 study explores three approaches which differ in how stomatal conductance is considered.

481

482 **3.1 Three approaches**

483 The three approaches are designed as follows:

484

485 Approach 1: This, we denote as the “*New Approach*”, is an implementation of the core of
 486 the present framework using two formulations for stomatal conductance as detailed in
 487 Sections 2.1 and 2.2, in which six unknowns, E_{tr} , g_{s,co_2} , A_n , c_i , ψ_l , and a' , are solved
 488 together (Figure 1a).

489 Approach 2: This uses LC-extended expression for stomatal conductance modeling, and
 490 that results in five unknowns, E_{tr} , g_{s,co_2} , A_n , c_i and ψ_l with five equations (Figure 1b). We
 491 call this approach “*LC-extended*”, of which a' is back-calculated from Eq. (16) after the
 492 five unknowns are solved and it is not a constant.

493 Approach 3: This uses the BBL-updated expression, Eq. (16), for stomatal conductance
 494 modeling and is referred to as the “*Semi-empirical*” approach. The parameter a' is treated
 495 as a constant with its values determined during model calibration. This also has five
 496 unknowns, E_{tr} , g_{s,co_2} , A_n , c_i , and ψ_l , to solve based on Eqs. (8)-(11) and (16).

497 With this setup, the *New Approach*, can be compared with the currently widely adopted
 498 methods of *Semi-empirical* and *LC-extended* approaches which work under water stressed
 499 conditions and for the latter the Prentice-2014 coordination hypothesis of $A_n = A_c = A_q$ is relaxed
 500 as well.

501 3.2 An implementation

502 With *New Approach* of the present modeling framework, we solve the six unknowns of
 503 E_{tr} , g_{s,co_2} , A_n , c_i , ψ_l , and a' by six equations, i.e., Eqs. (7)-(11) and Eq. (16). We have assigned
 504 ranges of search during optimization computation for g_{s,co_2} and a' in the following bounds,

$$505 \quad 0 \leq g_{s,co_2} \leq g_{s,co_2max} \quad (18)$$

506 and

$$507 \quad 0 \leq a' \leq a'_{max} \quad (19)$$

508 The upper bound of g_{s,co_2} is taken as $g_{s,co_2max} = 0.5 \text{ [mol}\cdot\text{m}^{-2}\cdot\text{s}^{-1}]$ which is based on the
 509 general observed physical maximum value for all of the vegetation types based on the literature

510 reported in Nobel (1999). The value of a'_{max} depends on the type of vegetation. Slopes in the
 511 original BBL model that a' is related to vary between 2 and 250 (Miner et al., 2017). In this
 512 study, a'_{max} are obtained through regression between the original BBL and the BBL-updated for
 513 different vegetation types (Clavijo Sanabria, 2020).

514 For the present *New Approach*, the problem to be solved is thus a constrained
 515 optimization problem. There are multiple ways of solving these six unknowns, Figure 1a describes
 516 one way of solving them. As for *LC-extended*, they are solved with Eqs. (7)-(11) as described in
 517 Figure 1b. Procedure of solving the five unknowns for the *Semi-empirical* is achieved by simply
 518 keeping a' constant following Luo et al. (2013).

519 For the optimality-based *New Approach*, the minimum cost criterion, $dCost/dc_i$, could be
 520 obtained via some optimization schemes but here we use an exhaustive search method which
 521 searches all possible c_i values at a regular interval to ascertain the global minimum is reached for
 522 in-depth discussion. The solution procedure starts with known soil water potential, ψ_{soil} , at the
 523 time step $t=1$ in Figure 1a. The main steps are briefly described below:

524 Step 1: Follow a sequential order and use the one in the queue of the equally spaced c_i for the
 525 current time step.

526 Step 2: Try a value of g_{s,co_2} from the range based on Eq. (18). Calculate g_s , E_{tr} , then ψ_l .

527 Step 3: Calculate A_n based on Eqs. (11) and (15) and express it as A_{n1} . Calculate the CO₂
 528 assimilation from the modified Farquhar model, i.e., Eqs. (10) and (12) – (14), and
 529 express it as A_{n2} (Figure 1a).

530 Step 4: Check the difference between A_{n1} and A_{n2} . If their difference, $|(A_{n2} - A_{n1})/A_{n1}|$, is greater
 531 than the threshold 10^{-10} , go back to Step 2 and select a new value for g_{s,co_2} and repeat
 532 until this threshold is met. If the tolerance is not met after the maximum number of
 533 iterations is reached, go back to Step 1 and select the next value of c_i .

534 Step 5: Calculate a' based on Eq. (16). If $a' > a'_{max}$ and the maximum number of iterations
 535 prescribed is not reached, go back to Step 1 and select the next value of c_i and start over.
 536 If the maximum number of iterations is reached, then stop. This study has not

537 encountered this scenario, however. If $a' \leq a'_{max}$, calculate and store the cost defined by
 538 Eq. (7a).

539 Step 6: Proceed to the next c_i and repeat Step 2 – Step 5 until all the equally spaced c_i between
 540 I^{*} and c_a are checked.

541 The c_i that produces the least cost, together with its associated E_{tr} , g_{s,CO_2} , A_n , ψ_l , and a' are the
 542 solution for the current time step.

543 When processes are considered simultaneously from different perspectives, they are
 544 coupled through shared variables. There is less “freedom” for these shared variables as they must
 545 conformed to different perspectives and thereby reduces the model uncertainty. In addition, this
 546 modeling framework can reduce the required number of model parameters that need to be
 547 calibrated. A case in point: here we solve ψ_l and c_i together with the leaf water potential (ψ_l)
 548 shared in Eqs. (9), (10), (12), (15), and (16), and CO₂ concentration within leaf (c_i) in Eqs. (7),
 549 (10), (11), (13), (14), and (16).

550 3.3 Two hydrological models used

551 Two hydrological models, VIC+ and DHSVM, that have significantly different model
 552 structures are employed and each is applied to two different locations to investigate the
 553 versatility and benefits of our modeling framework.

554 VIC+ (Luo et al., 2016; 2013) extends the Three-Layer Variable Infiltration Capacity
 555 (VIC-3L) large-scale hydrological model (Liang et al., 1994,1996a,1996b, 2003; Liang & Xie,
 556 2001, 2003) with important new features. The enhancement in VIC+ are as follows: First, VIC+
 557 considers hydraulic redistribution (HR) process and its effect on the interplay between plant
 558 transpiration and groundwater dynamics under water-limited conditions. Second, it explicitly
 559 represents groundwater table movement within the soil column and its tight interactions with the
 560 HR process. Third, it explicitly represents the photosynthesis process and its interactions with
 561 transpiration process. Fourth, it introduces our strategy into hydrological modeling by
 562 simultaneously representing the same process using multiple expressions from different
 563 perspectives to constrain the model. Fifth, VIC+ considers impact of plant storage on the water,

564 energy, and CO₂ cycles. In addition to these new features introduced to it, VIC+ also maintains
565 the original unique features included in the VIC-3L model (Liang et al., 1994, 1996a, 1996b,
566 2003, 2004; Liang and Xie, 2001, 2003; Cherkauer and Lettenmaier, 1999, 2003), such as
567 considering subgrid spatial variability of soil and vegetation properties and precipitation,
568 accounting for both infiltration and saturation excess runoff generation mechanisms for each
569 modeling grid in an interactive way under the context of subgrid spatial variability associated
570 with watershed properties (Liang and Xie, 2001; 2003). These original VIC features make the
571 VIC model more robust and less scale dependent as compared to other land surface models as
572 illustrated by different studies (e.g., Liang et al., 1996a, 2004; Konapala et al., 2020; Li et al.,
573 2011).

574 The small-scale Distributed Hydrology Soil and Vegetation Model (DHSVM) (Wigmosta
575 et al., 2002; 1994) was developed to numerically represent the effects of topography, soil type,
576 and vegetation on hydrological processes, such as plant transpiration, surface and subsurface
577 runoff, and snow process for small watersheds with high spatial resolution described by digital
578 elevation model (DEM) data. Unlike VIC+ in which the groundwater table is computed based on
579 the mixed form of Richards equation (Luo et al., 2013), DHSVM calculates its groundwater table
580 based on a simple conceptual approach. Also, DHSVM does not have the hydraulic
581 redistribution process represented either. In DHSVM, the water and energy budgets are solved
582 for each modeling grid cell which may contain an overstory canopy and an understory or bare
583 soil. DHSVM uses Penman-Monteith equation to calculate its plant transpiration and it does not
584 consider photosynthesis process, nor CO₂ assimilation. Thus, we have added these processes to
585 DHSVM in this study, and the modified DHSVM model is denoted as DHSVMm.

586 There are some conceptual model parameters and physically based model parameters
587 which cannot be well determined for either VIC+ or DHSVMm due to limited available
588 observations. Together there are eleven parameters needed to be calibrated for each model as
589 listed in Table 1: three are common to both, and if a' is posed as an unknown as in the *New*
590 *Approach* that number reduces to two. These parameters are manually calibrated for each

591 hydrological model using the *Semi-empirical* approach. The calibrated parameters are then kept
592 unchanged for use in the other two approaches.

593 3.4 Four study sites and calibration

594 The four study sites selected are all of plot-scales. The main reasons to choose the plot-
595 scale sites are because (1) the availability of observations, e.g., gross primary production (GPP),
596 latent heat flux, and soil moisture, are all of plot-scales; (2) fewer number of model parameters
597 need to be manually calibrated, and (3) the routing process and its associated routing parameters
598 do not need to be included and calibrated. This allows the major efforts of the analysis be
599 devoted to the focus of the study.

600 Since VIC+ includes the representation of hydraulic redistribution, groundwater and
601 surface water interaction, plant storage, and leaf water potential, it is applied to two forest sites
602 where impacts on fluxes due to deep roots under normal and water-limited conditions can be
603 effectively investigated. These two forest sites are the Duke Forest Loblolly Pine (US-Dk3)
604 located in North Carolina and the Blodgett Forest (US-Blo) located in California. The main
605 vegetation of the Duke forest is loblolly pine trees with different hardwood understory species.
606 Soil types are loam and clay. The mean annual precipitation is 1145 mm and the mean air
607 temperature is 15.5 °C. The hourly forcing data of years 2004 and 2005 at the Duke site are used
608 for calibration and validation, respectively. The Blodgett site is covered by mixed-evergreen
609 conifer forest with dominant even-aged ponderosa pine. Its primary soil type is loam. The mean
610 annual precipitation is 1226 mm and the mean air temperature is 11.1 °C. The hourly forcing data
611 of year 2004 at the Blodgett forest site are used for calibration. Since there are no complete
612 hourly forcing data available for other periods at the Blodgett site, no validation was carried out.
613 The seasonal precipitation distributions are different at the two forest sites. For the Duke forest
614 site, the dry period is short and distributed throughout the year. But for the Blodgett site, the dry
615 period is long and occurs over the summer months. Thus, plants at the Blodgett site survive the
616 summer through optimizing their behaviors and stored soil moisture to adapt to the dry climate
617 conditions.

618 The DHSVMm is applied to two grassland sites since its limitations are less severe for
619 grassland as discussed. These two are the Mather site located in Pennsylvania in USA and the

620 Oensingen site located in Switzerland. The Mather site is covered with alfalfa, white clover, red
 621 clover, and tall fescue grass. Its mean annual precipitation is 1148 mm with about 85
 622 precipitation days per year, and its mean annual temperature is 10 °C. The Mather site has a
 623 temperate continental climate with warm summers. The Oensingen site is covered with mixed-
 624 grasses. The mean annual precipitation is 1100 mm and the mean annual temperature is 9 °C.
 625 Hourly forcing data of the year 2010 are used at both grassland sites.

626 The main reason we use the *Semi-empirical* approach to carry out the calibration and
 627 validation is that it has the additional constant a' in its semi-empirical stomatal conductance
 628 model which needs to be calibrated. Results from the two hydrological models are shown in
 629 Figure 2. The observed data are from AmeriFluxin for Duke and Blodgett sites, and from
 630 MODIS for Mather and Oensingen sites.

631 Through regression between the original BBL and the BBL-updated for different
 632 vegetation types, we obtain for both the Duke and Blodgett sites, $a'_{max} = 9$, for the Mather site,
 633 $a'_{max} = 17$, and for the Oensingen site $a'_{max} = 24$. In *Semi-empirical*, a' is considered constant and
 634 $a' = 2$ is found to have the best fit for all four sites based on the manual calibrations in both
 635 VIC+ and DHSVMm.

636 The relative differences based on L2 norm (LD) and the coefficient of determination (R^2)
 637 for each observed variable are computed. From Figure 2, we can see that VIC+ simulates the soil
 638 moisture best, followed by latent heat flux, then the gross primary productivity (GPP); while
 639 DHSVMm simulates the GPP quite well. At the Duke site, for soil moisture, latent heat and GPP,
 640 their R^2 and LD (in parenthesis) are 0.87 (0.13), 0.83 (0.39) and 0.7 (0.47), respectively; and at
 641 the Blodgett site, they are 0.92 (0.12), 0.62 (0.54), and 0.60 (0.81). For the two grassland sites,
 642 total evapotranspiration (ET) and GPP are measured and DHSVMm consistently gives larger ET,
 643 but better estimates of GPP. For ET and GPP, their R^2 and LD for Mather are 0.79 (1.35) and
 644 0.88 (0.36), respectively; and 0.64 (1.21) and 0.87 (0.39) for Oensingen site. Considering the
 645 complexity of the modeling involved, these levels of relative difference with the limited
 646 measured data can be viewed as having reached reasonably good fit.

647 After the model calibrations, the cost function of Eq. (7) is employed to determine the
 648 ratio a/b needed. A sensitivity analysis between c_i/c_a and the different ratios of a/b for each of

649 the four sites is presented in Figure 3. The ratio of $a/b = 1/146 \approx 0.0068$ suggested by (Stocker
650 et al., 2020) based on data is also included in Figure 3 for comparison. All these four sites show
651 similar patterns – the value of c_i/c_a increases with a decrease in a/b . When a/b is between
652 0.001 and 1, the value of c_i/c_a is not sensitive to the a/b value at these four sites. Therefore, a/b
653 = 1/146, which is within the insensitive range for all these four sites, is used in this study.

654 **4. Results and analyses**

655 On the outset it is important to emphasize that for the present complex modeling problem
656 the available measurements related to plant behaviors are limited to only 3 and 2 variables,
657 respectively, for the forest sites and the grassland sites, and only one of the measurements is
658 directly related to a modeling variable, E_{tr} . Because of this limitation, a system with variables
659 incorrectly solved might still perform seemingly well with respect to the data – an equifinality
660 pitfall. Under this circumstance, what physical insights one approach can reveal over another
661 weigh more on the merits of different approaches than their goodness of fit to the few
662 measurements. This is particularly so as we are dealing with plausible expressions of the same
663 processes and, by nature, they give similar results with respect to the limited measurements in
664 order to be considered equally plausible.

665 4.1 Models versus available data

666 Results of *New Approach*, *LC-extended* and *Semi-empirical* approaches are first
667 compared with the limited available measurements. The latter two represent the current practice
668 albeit that *LC-extended* is an extension of Prentice-2014 to cover dry climates. All three
669 approaches using the same parameter values calibrated via *Semi-empirical*. Results from each
670 approach in comparison with the available observation data are shown through Figures 2, 4 and
671 5. Unsurprisingly, they all give compatible relative errors and goodness of fit to the data as the
672 results summarized in Figures 2, 4 and 5 illustrate. These plots include both daytime and
673 nighttime simulation results and observations. These results also show that the *LC-extended*

674 formulation developed in this study and used in *LC-extended* approach works for the dry weather
675 condition as intended.

676 4.2 Comparison of the solved variables

677 To gain deeper insights, we compare results of the main variables A_n , c_i , E_{tr} , ψ_l , g_{s,co_2} and
678 a' obtained from different approaches during the study period. Nighttime c_i , A_n , g_{s,co_2} , ψ_l , and E_{tr}
679 from sunset to 8am the next day are excluded from evaluation because at nighttime c_i approaches
680 c_a which results in the three variables of c_i , A_n , and E_{tr} having similar values among different
681 approaches and, if included, would skew the overall differences.

682

683 Before we start our detailed analyses and discussions, it is important to note that (1) a'
684 has not been treated as a variable in previous studies, (2) impacts of a' on other variables, A_n ,
685 c_i , E_{tr} , ψ_l , g_{s,co_2} are found significant, and (3) solutions of A_n , c_i , E_{tr} , ψ_l , g_{s,co_2} from *LC-extended*
686 are the same as those from *New Approach*, when the former gives $a' < a'_{max}$, but are very
687 different otherwise.

688

689 To show indeed each of the two different perspectives on stomatal conductance leads to
690 different results, we first compare *Semi-empirical* and *LC-Extended*. Their results presented in
691 Figure 6 do show significant difference.

692

693 To assess merits of the *New Approach*, pairwise comparisons are made. First, *New*
694 *Approach* vs *Semi-empirical* results plotted in Figure 7 show that their g_{s,co_2} , a' , c_i , and ψ_l are
695 significantly different at all four sites studied. Relative differences presented in Figure 8 provide
696 a sharper view of these comparisons. The largest relative differences happen in E_{tr} , ψ_l , g_{s,co_2} and
697 a' which can be as high as 100% except for ψ_l at the two grassland sites where the relative
698 differences can be as high as 200%, followed by c_i which can be up to 50%, while the
699 differences in A_n , generally less than 50% at all four sites, are the smallest. The dramatic
700 differences in a' occur because the *Semi-empirical* fails to consider the time-varying nature of a'
701 by keeping it constant. The constant $a' = 2$, determined through calibration, is much smaller
702 almost at all time than those obtained by *New Approach* during the study period as shown in

703 Figure 7. This implies that a' turns out to be a critical factor driving the differences in the
704 solution of other variables.

705 Comparisons between the *New Approach* and *LC-extended* are presented in Figures 8 and
706 9. For *LC-extended*, a' are back-calculated using Eq. (16) after A_n , g_{s,CO_2} , c_i , and ψ_l are solved.
707 Their relative differences (Figure 8) are the lowest in A_n among the six variables at the two forest
708 sites, and are comparable between A_n and c_i at the two grassland sites. At all four sites,
709 differences in E_{tr} are similar to those between *New Approach* and *Semi-empirical* but with less
710 scatter. We note that the largest relative differences in E_{tr} between *New Approach* and *LC-*
711 *extended* are greater than those between the *New Approach* and *Semi-empirical*; furthermore,
712 13.6% (Duke), 18.4% (Blodgett), 15.9% (Mather), and 7.6% (Oensingen) of the data lie outside
713 the bounds of Figure 8. Also, E_{tr} estimates from the *New Approach* are generally greater than
714 those from *Semi-empirical* at all four sites, while mostly smaller than those from *LC-extended*
715 (Figure 8). The differences in c_i are smaller than those between *New Approach* and *Semi-*
716 *empirical* except for the summer months at the Blodgett site where the differences are larger.
717 Similar to E_{tr} , the c_i estimates from the *New Approach* are also generally greater than those from
718 *Semi-empirical* at all four sites, while mostly smaller than those from *LC-extended* (Figure 8).
719 For ψ_l , even though the largest differences between the *New Approach* and *LC-extended* are
720 larger than those between *New Approach* and *Semi-empirical*, the majority of the differences are
721 smaller as indicated by the LD metric for the two forest sites; as for the two grassland sites, the
722 differences between the *New Approach* and *LC-extended* are much smaller than those between
723 *New Approach* and *Semi-empirical* (Figures 7, 8, and 9). The relative differences between *New*
724 *Approach* and *LC-extended* that lie outside the bounds of Figure 8 for ψ_l is 9.3% for the Mather
725 site and 5.2% for the Oensingen site, respectively. On the other hand, the relative differences
726 between *New Approach* and *Semi-empirical* that lie outside the displayed bounds for ψ_l are
727 17.7% and 59.2% for the Mather and Oensingen sites, respectively. Values in ψ_l and E_{tr} from
728 *LC-extended* (Figures 8 and 9) are also closer to those from *New Approach* than from *Semi-*
729 *empirical* (Figures 78, and 9) at all four sites. Similar to E_{tr} and c_i , estimates in ψ_l from the *New*
730 *Approach* are also generally smaller than those from *LC-extended*, while they are mostly larger
731 than those from *Semi-empirical* (Figure 8) at both forest sites. For the two grassland sites,
732 however, estimates in ψ_l from the *New Approach* are generally smaller than those from both *LC-*

733 *extended* and *Semi-empirical*. These general patterns are, in fact, associated with the large
 734 differences in g_{s,co_2} and a' among the three approaches further discussed next.

735 In terms of the relative differences in A_n , c_i , E_{tr} , and ψ_l , (see Figure 8), the largest
 736 differences still reside in E_{tr} and ψ_l , followed by c_i , with the smallest in A_n at all four sites,
 737 although the differences in c_i and A_n are comparable at the two grassland sites. Comparing the
 738 relative differences between *New Approach* and *Semi-empirical*, those between *New Approach*
 739 and *LC-extended* are generally smaller at all four sites. However, the differences in g_{s,co_2} and a'
 740 are pronounced (Figures 8 and 9), and the trend of the differences in g_{s,co_2} and a' is reversed
 741 from that between *LC-extended* versus *Semi-empirical*. For both g_{s,co_2} and a' the *New Approach*
 742 gives much higher values than *Semi-empirical* (see Figures 7 and 8) but much lower values than
 743 *LC-extended* (see Figures 8 and 9) at all four sites. This is because a large number of a' are
 744 unrealistically high for all four sites with the *LC-extended*. For Duke, Blodgett, Mather, and
 745 Oensingen sites, there are, respectively, 45.7%, 79.1%, 49.4% and 44.9% of a' that are higher
 746 than a'_{max} (see Table 2a). These unreasonable a' values imply that using the minimum cost
 747 function, i.e., Eq. (7), together with other Eqs. (8) – (11), leaves a' an unmodeled free variable,
 748 and that introducing additionally Eq. (16) is necessary, even though the levels of differences in
 749 A_n , E_{tr} , c_i , and ψ_l between these two approaches are generally much smaller than those in g_{s,co_2}
 750 and a' between the *New Approach* and *LC-extended*. In fact, there are some a' values in the *LC-*
 751 *extended* that are higher than 200 at all four sites which are out of the display bound in Figure 9.
 752 Also, there are large percentages of relative differences between *New Approach* and *LC-extended*
 753 for g_{s,co_2} and a' whose values are outside their respective bounds displayed in Figure 8. For
 754 g_{s,co_2} , these percentages are, respectively, 29.9% (Duke), 32.3% (Blodgett), 32.6% (Mather), and
 755 17.2% (Oensingen). Further examination on a' is given below. Figures 8 and 9 clearly show that
 756 the differences in A_n , E_{tr} , c_i , and ψ_l are much smaller than those in g_{s,co_2} and a' between the *New*
 757 *Approach* and *LC-extended*, but these smaller differences are produced at the expense of
 758 unrealistic a' . This is an example of variable equifinality.

759 After studying these comparisons, it is clear that a' is a discriminant factor that explains
 760 the observed differences. In *LC-extended*, a' is an unmodeled free variable, and if $a' < a'_{max}$,

761 which happens 54.3% (Duke), 20.9% (Blodgett), 50.6% (Mather), and 55.1% (Oensigen) of the
 762 time, *New Approach* and *LC-extended* give same A_n , c_i , E_{tr} , ψ_l , g_{s,co_2} and a' . But for the rest of
 763 the time when $a' > a'_{max}$, results are very different. In this case, *LC-extended* gives solutions that
 764 consist of unreasonable five variable combinations—this is further detailed in the next section.
 765 As for the *Semi-empirical*, because a' is held constant, it yields even larger differences with the
 766 *New Approach*. Introducing a' as an additional modeled variable in the *New approach* is thus
 767 important and necessary.

768 Impact of a' , either from the unmodeled thus unconstrained a' in *LC-extended*, or from
 769 the inadequate treatment of a' as a constant from model calibration in *Semi-empirical*, is not
 770 known previously, and is an important investigation of this study.

771 4.3 Why a' should be a model variable

772 In this section we will show that consider a' as an additional model variable and set $a' \leq$
 773 a'_{max} has important implications. We will further show via analyzing *LC-extended* results that a'
 774 being a free variable lead to a large percentage of results having $a' > a'_{max}$ as summarized in
 775 Table 2a, and that those solutions having $a' > a'_{max}$ are predominantly unreasonable in light of
 776 physical reality as shall be presented in Table 2g. In contrast, by taking up a' as a model
 777 variable, such a serious problem is greatly reduced (Table 2h).

778 Eq (16) provides a clue as to when a' could be high in *LC-extended*. The solved A_n , c_i , ψ_l ,
 779 g_{s,co_2} results corresponding to $a' > a'_{max}$ are loosely parsed into four groups based on Eq. (16):
 780 (1) $g_{s,co_2} > 0.3$ mol/m²/s (red), (2) $\psi_l < -2.2$ MPa (blue), (3) $A_n < 2$ (green) and (4) $c_i > 300$
 781 (orange). Each group by itself does not mean much, however, a daytime (defined to be from 8
 782 AM to sunset in this study) result is deemed unrealistic if it falls into more than one of these four
 783 groupings as explained below. The intent here is not to define a rigorous boundary, but to
 784 explain how one can determine results to be unreasonable and slight variations on these
 785 boundaries would not affect the conclusions.

786 The *LC-extended* results having $a' > a'_{max}$ are presented in Figure 10a (forest sites) and
 787 Figure 10c (grassland sites) distinguished by the above grouping, while results that do not belong

788 to these four groups but have $a' > a'_{max}$ are also plotted (in grey). Table 2b lists the percentage of
 789 each group showing that these four groups indeed contribute most to $a' > a'_{max}$. Since they are
 790 not mutually exclusive from one another, the sum of them is more than 100%, indicating that
 791 there are points belonging to multiple groups at the same time. This is of significance as this is
 792 how we are able, guided by Figure 10, to pinpoint the problems of unreasonableness with those
 793 results having $a' > a'_{max}$. Take for example the combination of $A_n < 2 \mu\text{mol}/\text{m}^2/\text{s}$ and $c_i > 300$
 794 $\mu\text{mol}/\text{mol}$ (exclude those with small g_{s,co_2} which may be potentially reasonable), such
 795 combination is unlikely when their corresponding g_{s,co_2} values are not small (see orange dots in
 796 Figures 10b and 10d), for during daytime $c_i > 300 \mu\text{mol}/\text{mol}$ means photosynthesis activity is
 797 strong, and net carbon assimilation should be high, and thus $A_n < 2 \mu\text{mol}/\text{m}^2/\text{s}$ is unlikely and
 798 thus the set of solution should be discarded. The solutions having $\psi_l < -2.2$ with either $g_{s,co_2} > 0.3$
 799 or $c_i > 300$ and $g_{s,co_2} > 0.3$ and $A_n < 2$ can be similarly discounted. The combination of $\psi_l < -2.2$
 800 and $A_n < 2$ is found associated with large c_i (close to $300 \mu\text{mol}/\text{mol}$) (see Figure 10b) which is
 801 unrealistic. The combination of $g_{s,co_2} > 0.3 \text{ mol}/\text{m}^2/\text{s}$ and $c_i > 300 \mu\text{mol}/\text{mol}$ in daytime is possible,
 802 however, Figures 10b and 10d show that points in this group are associated mostly with small to
 803 medium A_n (although $A_n > 2$) under not water stressed conditions (in contrast to larger A_n values
 804 shown in Figure 9 at all four sites). Such a combination makes them unreasonable since with
 805 large g_{sco2} and large c_i , the assimilation A_n should be high as well in the daytime when they are
 806 not water stressed. Following such a detailed examination, we found that *LC-extended* results are
 807 unreasonable when they fall into any of the two-combinations of Table 2c. It then follows, three-
 808 combinations of Table 2d also are unreasonable based on similar reasoning discussed for the
 809 two-combinations in Table 2c. There is no result that simultaneously satisfies the four-
 810 combinations.

811 From Table 2c, data points satisfying both $A_n < 2 \mu\text{mol}/\text{m}^2/\text{s}$ and $c_i > 300 \mu\text{mol}/\text{mol}$
 812 constitute the largest fraction of two-group combination (except for the Oensingen Site) that
 813 leads to $a' > a'_{max}$ with 32.9% for Duke site, 14.7% for Blodgett site, 35.2% for Mather site, and
 814 20.8% for Oensingen site. That is to say, since a' is a free variable as in *LC-extended*, large c_i in
 815 daytime is often accompanied by unrealistically low A_n in order to achieve reasonable values of
 816 g_{s,co_2} (see Figures 10b and 10d) as observed from Eq. (16) as such combination would lead to the

817 optimal cost. With Eq. (16) added, however, A_n can no longer be very small as a' cannot be very
 818 large to compensate the very small A_n .

819 The grassland sites, comparing with the forest sites, are less water stressed for their ψ_l are
 820 always higher than -2.2 MPa. In less water stressed environments, the interactions between c_i
 821 and A_n and between g_{s,co_2} and c_i over the specified ranges are stronger for the combinations of
 822 $g_{s,co_2} > 0.3 \text{ mol/m}^2/\text{s}$ and $c_i > 300 \text{ } \mu\text{mol/mol}$ and of $c_i > 300 \text{ mol/m}^2/\text{s}$ and $A_n < 2$ account for much
 823 higher percentages at the grassland sites than at the forest sites (see Table 2c). Other than that,
 824 the four sites exhibit similar trends as can be seen in Figure 10.

825 Table 2c summarizes six possible 2-combinations of the 4 groupings while Table 2d
 826 shows four possible 3-combinations of the 4 groupings. Each of the rows of Table 2c plus Table
 827 2d does not sum up to 100% leading to an important question: might the results represented by
 828 other possible combinations be unreasonable as well? Further analysis is carried out to answer
 829 this question. First, we determine the percentage of results that only falls within one group
 830 (Table 2e) and not to any other three groups listed in Table 2e, and then further divide each
 831 group into subgroups. The difference between groups shown in Table 2e and those in Table 2b is
 832 that in Table 2e, the results in one column do not appear in another column, whereas it is not the
 833 case for Table 2b. In other words, results in each group shown in Table 2e do not overlap with
 834 any other groups. For groups in Table 2e, they are further divided into subgroups shown in
 835 Table 2f. Based on the behaviors of the plants and the observed data (e.g., Deans et al., 2020;
 836 Ennahli & Earl, 2005; Joshi et al., 2020; Leuning, 1995; Schulze & Hall, 1982; Urban et al.,
 837 2014; Zhou et al., 2013), those variable values having combinations fallen into these subgroups
 838 in Table 2f are identified as unreasonable. Using these added criteria, the fraction of data points
 839 within each subgroup of the unreasonable results is summarized in Table 2f. A total summation,
 840 together with Tables 2c and 2d, gives the total fraction of unreasonable results for those with
 841 $a' > a'_{max}$ in Table 2g. The results so obtained show that at least 70.9% for the forest sites and
 842 could be as high as 98.1% for grassland sites of all $a' > a'_{max}$ results are deemed unreasonable.
 843 We note that what this analysis shows is that we are not trying to conduct an exhaustive search

844 for all unreasonable variable combinations associated with $a' > a'_{max}$, but to show that there is a
 845 large fraction of them that is unreasonable.

846 But then there is a question that has to be addressed: are the results from *New approach*
 847 where $a' \leq a'_{max}$ all reasonable? Following the same analysis we have calculated its fraction of
 848 the unreasonable results, and find that they are much lower and are in the range between 3.2% to
 849 9.3% as shown in Table 2h. This represents a dramatic improvement. It, nonetheless, also points
 850 out that the current understanding still has room to improve.

851 In addition, in terms of what we have obtained with *New Approach* on the variation of a'
 852 values, our results (Figure 9) have shown that a' varied in a narrower range over time than those
 853 from *LC-extended*, and definitely not a constant. The a' values from *LC-extended* have a much
 854 larger variation range over the different periods of a year at all four sites. Specifically, for the
 855 *New Approach* the ranges of the hourly a' obtained for the two forest sites are, respectively,
 856 between 1.38 and 9 (Duke site, Figure 9g) over the two-year period and between 0.89 and 9
 857 (Blodgett site, Figure 9s) over one-year period; for the two grassland sites, it is between 1.79 and
 858 17 (Mather site, Figure 9ee) and between 2.15 and 24 (Oensingen site, Figure 9qq). In contrast,
 859 for the *LC-extended* approach the hourly a' varies between 1.36 and 800 (Duke) and between 0.8
 860 and 2270 (Blodgett) for the forest sites; and for the grassland sites between 1.79 and 313
 861 (Mather) and between 2.15 and 191 (Oensingen). Furthermore, *New approach* gives much
 862 narrower diurnal a' variation than *LC-extended* at both forest sites (see Figures 11g and 11o) and
 863 at the two grassland sites (Figure not shown)—which agrees well with the current data and
 864 understanding of a' (Miner et al., 2017).

865 The limited data available at present time only allow us to state that g_{s,co_2} , A_n , c_i , and ψ_l
 866 combinations are more reasonable with our *New Approach* based on plants general behaviors in
 867 the daytime and the observed data shown in the literature. Additionally, the time-varying a' from
 868 our *New Approach* removes the need of constant assumption, and from which one can easily
 869 estimate values of g_l based on Eq. (17) which is related to $\lambda = \partial A_n / \partial E_{tr}$ used in the optimality rule
 870 for the WUE group (e.g., Medlyn et al., 2011). In other words, one no longer needs to calibrate
 871 g_l or λ at each daily time step as is currently done in practice. Figures 11h and 11p show the
 872 comparisons of g_l 's among the three approaches over a summer week at both forest sites. In

873 Figure 11, comparisons on variables of g_{s,co_2} , A_n , c_i , ψ_l , and a' , together with E_{tr} and GPP where
 874 observations are available, are also included.

875 Results presented in Figures 6 - 11 demonstrate that, for all six solved variables, E_{tr} , A_n ,
 876 c_i , ψ_l , a' and g_{s,co_2} , our *New Approach*, which simultaneously employs two stomatal conductance
 877 models are significantly different from those using only either one. Furthermore, these results
 878 demonstrate that the differences between *Semi-empirical* and *LC-extended* (Figure 6) are larger
 879 than those between our *New Approach* and either *Semi-empirical* (Figure 7) or *LC-extended*
 880 (Figure 9) based on both metrics, R^2 and LD. These results clearly show that our *New Approach*
 881 takes the advantage of both models, *LC-extended* and *Semi-empirical*.

882 The preceding results show that only the *New Approach* gives reasonable values of a' and
 883 with it reasonable solutions, and that the problem studied is better described as having six
 884 variables.

885 4.4 Relationship between carboxylation and transpiration

886 The cost function, Eq. (7), represents a trade-off between carboxylation and transpiration.
 887 The relationship between carboxylation and transpiration is shown in Figure 12 in which
 888 carboxylation is presented by $V = V_{cmax}/A_n$, and transpiration is presented by $G = g_{sab,co_2}/A_n$.
 889 Prentice et al. (2014) showed that the $V \sim G$ relationship follows a hyperbola shape based on
 890 observed data with the observed V in the range between 0 and 30, and the observed G in the
 891 range between 0 and 0.05. Although their data are from instant measurements under certain
 892 conditions while here our modeling gives hourly results over one or two years, such a hyperbola
 893 relationship between V and G does provide another baseline to evaluate the results obtained.
 894 Figure 12 shows that results from both *New Approach* and *LC-extended* generally follow the
 895 hyperbola shape at all four sites, while the *Semi-empirical* does not, even though they have the
 896 same goodness of fit to the available data (see Figures 2, 4, and 5). Between *New Approach* and
 897 *LC-extended*, the former has less scatter, and a larger percentage of its results fall inside the
 898 range of $0 < G \leq 0.05$ [$\text{mol} \cdot \mu\text{mol}^{-1}$] and $0 < V \leq 30$ [$\text{mol} \cdot \text{mol}^{-1}$] (see Table 3). The larger scatter in
 899 the *LC-extended* in Figure 12 is due to its larger g_{s,co_2} and a' (see Figures 8 and 9) that result in
 900 larger G at all four sites, since the differences in A_n from both approaches are much smaller. On

901 the other hand, the reason that the *Semi-empirical* approach does not show hyperbola $V \sim G$
 902 relationship is because g_{s,co_2} are constrained to small values (see Figure 7) by the use of a
 903 constant $a' = 2$ from calibration. Not having a dynamic a' imposes limitations on the *Semi-*
 904 *empirical* approach.

905 **5. Conclusions**

906 In this study, we present a modeling framework which is applied to model the water and
 907 carbon exchange of plants inside hydrological models. We have demonstrated how we pose six
 908 equations, i.e., Eqs. (7) – (11) and Eq. (16), and two constraints (18) and (19) to solve a
 909 constrained optimization problem of six variables, E_{tr} , g_{s,co_2} , A_n , c_i , ψ_l , and a' . The core idea of
 910 this modeling framework is to model processes that are important and yet not completely
 911 understood with multiple equally plausible expressions from different perspectives. This
 912 represents an extension of the modeling strategy proposed in VIC+ by Luo et al. (2016; 2013). In
 913 the process, we have also extended the minimum cost optimality rule of Prentice et al. (2014) so
 914 that it applies to water-limited conditions. The extension also relaxes the coordination
 915 assumption that the Rubisco-limited photosynthetic rate be equal to electron transport-limited
 916 photosynthetic rate.

917 The unique strength of this modeling framework includes the following: First, not only
 918 does this modeling framework provide more constraints to the same process to reduce the
 919 modeling system's free variables and unreasonable variable value combinations, but also
 920 individual processes are more comprehensively described because they are represented from
 921 multiple perspectives. Second, the presence of various constraints makes the individual processes
 922 more tightly coupled through shared variables which are solved simultaneously.

923 To further shed light on the impacts of the present framework, we conduct comparative
 924 studies employing two currently widely used stomatal conductance models. Three approaches
 925 used are denoted as: *New Approach* (the present model), *LC-extended* and *Semi-empirical*. To
 926 illustrate the versatility of the framework, this study uses two different hydrological models and
 927 four different study sites: VIC+ on two forest sites and the modified DHSVMm on two grassland
 928 sites. Our results show that all three approaches give compatible results regarding the available
 929 limited observation data. But a close examination shows that the differences in the solved

930 variables E_{tr} , A_n , c_i , g_{s,co_2} , ψ_l and a' are significant. This is a well-known phenomenon called
931 equifinality that in modeling a complex system that the “right” results may be obtained with
932 wrong solutions when observation data are limited. In-depth investigation reveals that the
933 differences among the variables can be attributed to the treatment of a' : *Semi-empirical* treats it
934 as a constant; *LC-extended* treats it as a free variable by not considering it; and the present *New*
935 *Approach* considers it as a modeling variable. The *New Approach* with two stomatal conductance
936 models fused together is able to solve a' that agrees with the current understanding obtaining
937 nearly constant day time a' and how the a' values vary between days. This indicates that *Semi-*
938 *empirical* using a constant a' throughout a study period is not desirable, and that *LC-extended*
939 not considering it at all which would result in a high fluctuation of a' over a diurnal cycle (see
940 Figures 11g and 11o) is not desirable either. Furthermore, results from *New Approach* give
941 hyperbolic relationship between plant carboxylation and transpiration as field observation
942 dictates which further indirectly provides merits to the proposed framework as it matches with
943 the trend observed.

944 Our investigation into the reasonableness of results in terms of physical reality has shown
945 that the *New approach*, albeit makes dramatic improvements in this respect, still gives some
946 unreasonable variable combinations, albeit a much smaller fraction, in the results. This reflects
947 that there still exists some knowledge gap in the current understanding and expressions, and
948 more work needs to be done.

949 It is also worth mentioning that the *New Approach* presented is simply one
950 implementation of our modeling framework. The core idea of including as many least overlapped
951 equally plausible or quasi-equally plausible formulations as possible can constrain a modeling
952 system, reduce model's free variables and mitigate equifinality, decrease result uncertainties, and
953 ultimately increase the model robustness and predictability – very important characteristics a
954 model should possess (Prentice et al., 2015). This strategy also enables the modeling system to
955 have more unknowns solved simultaneously, and thus makes it possible to have the different
956 expressions in the model interact with and depend on one another. Plausible expressions for the
957 same process obtained via different perspectives, when properly introduced, complement one
958 another. This is why our modeling framework can make the system more robust and stable when
959 the unknown variables of the system are solved in such a manner. Our results with two different

960 hydrological models, VIC+ and DHSVMm, applied to four different locations, clearly
961 demonstrate these points. That is, results from our framework – the *New Approach* – provide not
962 only good estimates on E_{tr} , A_n , c_i , and ψ_p , but also more reasonable values on g_{s,co_2} and a' , and
963 the hyperbolic V~G shape as well.

964 Our modeling framework could also facilitate identification of inconsistency, should it
965 exist, among the different quasi-equally plausible expressions. This is because if no reasonable
966 solutions could be obtained by solving simultaneously all of the unknowns of the system, it could
967 imply that some of these expressions were not compatible with each other. In this way, by
968 analyzing the results, one may be provided with new insight regarding what could be the terms
969 or factors that may be missing, and under what conditions these expressions may not be
970 compatible, while at other conditions they are compatible and complement each other. After all,
971 the ecosystem is such a complex system, our current understanding of the system and the
972 available observations may not yet provide us processes that could fully describe the nature. This
973 modeling framework could help us move forward in identifying the gaps.

974 Lastly, our modeling strategy is not only applicable to the hydrological models (e.g.,
975 VIC+ and DHSVMm), but also suitable to other modeling systems in other fields where
976 knowledge is incomplete and many models from different perspectives are equally or quasi-
977 equally plausible. With the advance of our understanding and knowledge of the various complex
978 natural processes, more constraints/equations/expressions will be discovered, and they can be
979 fused together in a fashion similar to what we do here in studying the soil-plant-atmosphere
980 continuum. This study shows how this modeling framework can be realized, tested, and
981 explored.

982

983 **Acknowledgements:**

984 This work was partially supported by the U.S. National Science Foundation under CBET-
985 1236403 to the University of Pittsburgh, the LEMONTREE (Land Ecosystem Models based On
986 New Theory, obseRvations and ExperimEnts) project funded through the generosity of Eric and
987 Wendy Schmidt by recommendation of the Schmidt Futures program, and by the William Kepler

988 Whiteford Professorship to Xu Liang from the University of Pittsburgh. We also thank the
989 Center for Research Computing and the Swanson School of Engineering for providing the
990 computational resources at the University of Pittsburgh. We are indebted to Professor I. Colin
991 Prentice of Imperial College London for his generosity in sharing insights and expertise on
992 optimality models.

993

994 **Author contributions:**

995 For this work, Liuyan Hu and Hector W. Clavijo implemented the research ideas, performed
996 model simulation experiments with Hu for the VIC+ model and Clavijo for the DHSVMm
997 model, respectively, conducted analysis, and contributed to the manuscript writing at the
998 beginning. Liuyan Hu prepared all the tables and figures. Jeen-Shang Lin contributed to the
999 result analyses and coauthored the final manuscript. Xu Liang conceived the research ideas,
1000 designed the model simulation experiments, supervised the investigation, synthesized the results,
1001 and wrote and finalized the manuscript. All contributed to the discussions of the work.

1002

1003 **Data access:**

1004 Data utilized in this study are accessible from the Ameriflux at <https://ameriflux.lbl.gov/>, from
1005 Euroflux at <http://www.europe-fluxdata.eu/>, from NASA MODIS at
1006 <https://lpdaacsvc.cr.usgs.gov/appears/>. All the data generated in this work for the figures and
1007 tables will be available through Mendeley Data (DOI: xxx). The VIC
1008 (<https://vic.readthedocs.io/en/master/>) and DHSVM (<https://dhsvm.pnnl.gov/>) models are all
1009 open sources.

1010

1011 **References:**

1012 Anderegg, W. R., Wolf, A., Arango-Velez, A., Choat, B., Chmura, D. J., Jansen, S., et al. (2018). Woody plants
1013 optimise stomatal behaviour relative to hydraulic risk. *Ecology letters*, 21(7), 968-977.

- 1014 Ball, J. T., Woodrow, I. E., & Berry, J. A. (1987). A model predicting stomatal conductance and its contribution to
 1015 the control of photosynthesis under different environmental conditions. In *Progress in photosynthesis*
 1016 *research* (pp. 221-224): Springer.
- 1017 Bauerle, W. L., & Bowden, J. D. (2011). Predicting transpiration response to climate change: insights on
 1018 physiological and morphological interactions that modulate water exchange from leaves to canopies.
 1019 *HortScience*, 46(2), 163-166.
- 1020 Berry, J. A., Beerling, D. J., & Franks, P. J. (2010). Stomata: key players in the earth system, past and present.
 1021 *Current opinion in plant biology*, 13(3), 232-239.
- 1022 Beven, K. (2006). A manifesto for the equifinality thesis. *Journal of hydrology*, 320(1-2), 18-36.
- 1023 Buckley, T. N., Sack, L., & Farquhar, G. D. (2017). Optimal plant water economy. *Plant, cell & environment*, 40(6),
 1024 881-896.
- 1025 Cherkauer, K. A., & Lettenmaier, D. P. (1999). Hydrologic effects of frozen soils in the upper Mississippi River
 1026 basin. *Journal of Geophysical Research: Atmospheres*, 104(D16), 19599-19610.
- 1027 Cherkauer, K. A., & Lettenmaier, D. P. (2003). Simulation of spatial variability in snow and frozen soil. *Journal of*
 1028 *Geophysical Research: Atmospheres*, 108(D22).
- 1029 Clavijo Sanabria, H. W. (2020). *An Investigation on Interactions between Plant Physiological-Hydrological-*
 1030 *Biogeochemical processes and Acid Mine Drainage in Coal Refuse Piles using Optimality Principle*
 1031 *Theory*. University of Pittsburgh,
- 1032 Collatz, G. J., Ball, J. T., Grivet, C., & Berry, J. A. (1991). Physiological and environmental regulation of stomatal
 1033 conductance, photosynthesis and transpiration: a model that includes a laminar boundary layer.
 1034 *Agricultural and Forest meteorology*, 54(2-4), 107-136.
- 1035 Collatz, G. J., Ribas-Carbo, M., & Berry, J. (1992). Coupled photosynthesis-stomatal conductance model for leaves
 1036 of C4 plants. *Functional Plant Biology*, 19(5), 519-538.
- 1037 Cowan, I. (1982). Regulation of water use in relation to carbon gain in higher plants. In *Physiological plant ecology*
 1038 *II* (pp. 589-613): Springer.
- 1039 Cowan, I., & Farquhar, G. (1977). Stomatal function in relation to leaf metabolism and environment.
- 1040 Daly, E., Porporato, A., & Rodriguez-Iturbe, I. (2004). Coupled dynamics of photosynthesis, transpiration, and soil
 1041 water balance. Part I: Upscaling from hourly to daily level. *Journal of Hydrometeorology*, 5(3), 546-558.
- 1042 Damour, G., Simonneau, T., Cochard, H., & Urban, L. (2010). An overview of models of stomatal conductance at
 1043 the leaf level. *Plant, cell & environment*, 33(9), 1419-1438.
- 1044 De Kauwe, M. G., Zhou, S., Medlyn, B. E., Pitman, A. J., Wang, Y., Duursma, R. A., & Prentice, I. C. (2015). Do
 1045 land surface models need to include differential plant species responses to drought? Examining model
 1046 predictions across a mesic-xeric gradient in Europe.
- 1047 Deans, R. M., Brodribb, T. J., Busch, F. A., & Farquhar, G. D. (2020). Optimization can provide the fundamental
 1048 link between leaf photosynthesis, gas exchange and water relations. *Nature Plants*, 6(9), 1116-1125.
- 1049 Dewar, R., Mauranen, A., Mäkelä, A., Hölttä, T., Medlyn, B., & Vesala, T. (2018). New insights into the covariation
 1050 of stomatal, mesophyll and hydraulic conductances from optimization models incorporating nonstomatal
 1051 limitations to photosynthesis. *New Phytologist*, 217(2), 571-585.
- 1052 Eller, C. B., Rowland, L., Oliveira, R. S., Bittencourt, P. R., Barros, F. V., da Costa, A. C., et al. (2018). Modelling
 1053 tropical forest responses to drought and El Niño with a stomatal optimization model based on xylem
 1054 hydraulics. *Philosophical Transactions of the Royal Society B: Biological Sciences*, 373(1760), 20170315.
- 1055 Ennahli, S., & Earl, H. J. (2005). Physiological limitations to photosynthetic carbon assimilation in cotton under
 1056 water stress. *Crop Science*, 45(6), 2374-2382.
- 1057 Farquhar, G. D., von Caemmerer, S. v., & Berry, J. A. (1980). A biochemical model of photosynthetic CO₂
 1058 assimilation in leaves of C₃ species. *Planta*, 149(1), 78-90.
- 1059 Feynman, R. (1967). *The character of physical law*: First MIT Press Paperback Edition.
- 1060 Franklin, O., Johansson, J., Dewar, R. C., Dieckmann, U., McMurtrie, R. E., Brännström, Å., & Dybzinski, R.
 1061 (2012). Modeling carbon allocation in trees: a search for principles. *Tree Physiology*, 32(6), 648-666.
- 1062 Gutschick, V., & Simonneau, T. (2002). Modelling stomatal conductance of field-grown sunflower under varying
 1063 soil water content and leaf environment: comparison of three models of stomatal response to leaf
 1064 environment and coupling with an abscisic acid-based model of stomatal response to soil drying. *Plant, Cell*
 1065 *& Environment*, 25(11), 1423-1434.
- 1066 Heroult, A., LIN, Y. S., Bourne, A., Medlyn, B. E., & Ellsworth, D. S. (2013). Optimal stomatal conductance in
 1067 relation to photosynthesis in climatically contrasting Eucalyptus species under drought. *Plant, Cell &*
 1068 *Environment*, 36(2), 262-274.

- 1069 Hölttä, T., Lintunen, A., Chan, T., Mäkelä, A., & Nikinmaa, E. (2017). A steady-state stomatal model of balanced
1070 leaf gas exchange, hydraulics and maximal source–sink flux. *Tree physiology*, 37(7), 851-868.
- 1071 Jarvis, P. (1976). The interpretation of the variations in leaf water potential and stomatal conductance found in
1072 canopies in the field. *Philosophical Transactions of the Royal Society of London. B, Biological Sciences*,
1073 273(927), 593-610.
- 1074 Joshi, J., Stocker, B. D., Hofhansl, F., Zhou, S., Dieckmann, U., & Prentice, I. C. (2020). Towards a unified theory
1075 of plant photosynthesis and hydraulics. *BioRxiv*.
- 1076 Katul, G., Manzoni, S., Palmroth, S., & Oren, R. (2010). A stomatal optimization theory to describe the effects of
1077 atmospheric CO₂ on leaf photosynthesis and transpiration. *Annals of Botany*, 105(3), 431-442.
- 1078 Katul, G., Palmroth, S., & Oren, R. (2009). Leaf stomatal responses to vapour pressure deficit under current and
1079 CO₂-enriched atmosphere explained by the economics of gas exchange. *Plant, Cell & Environment*, 32(8),
1080 968-979.
- 1081 Konapala, G., Kao, S. C., & Addor, N. (2020). Exploring Hydrologic Model Process Connectivity at the Continental
1082 Scale Through an Information Theory Approach. *Water Resources Research*, 56(10), e2020WR027340.
- 1083 Leuning, R. (1990). Modelling stomatal behaviour and photosynthesis of Eucalyptus grandis. *Functional Plant
1084 Biology*, 17(2), 159-175.
- 1085 Leuning, R. (1995). A critical appraisal of a combined stomatal-photosynthesis model for C₃ plants. *Plant, Cell &
1086 Environment*, 18(4), 339-355.
- 1087 Leuning, R., Dunin, F., & Wang, Y.-P. (1998). A two-leaf model for canopy conductance, photosynthesis and
1088 partitioning of available energy. II. Comparison with measurements. *Agricultural and Forest Meteorology*,
1089 91(1-2), 113-125.
- 1090 Li, H., Huang, M., Wigmosta, M. S., Ke, Y., Coleman, A. M., Leung, L. R., et al. (2011). Evaluating runoff
1091 simulations from the Community Land Model 4.0 using observations from flux towers and a mountainous
1092 watershed. *Journal of Geophysical Research: Atmospheres*, 116(D24).
- 1093 Liang, X., Guo, J., & Leung, L. R. (2004). Assessment of the effects of spatial resolutions on daily water flux
1094 simulations. *Journal of Hydrology*, 298(1-4), 287-310.
- 1095 Liang, X., Lettenmaier, D. P., & Wood, E. F. (1996). One-dimensional statistical dynamic representation of subgrid
1096 spatial variability of precipitation in the two-layer variable infiltration capacity model. *Journal of
1097 Geophysical Research: Atmospheres*, 101(D16), 21403-21422.
- 1098 Liang, X., Lettenmaier, D. P., Wood, E. F., & Burges, S. J. (1994). A simple hydrologically based model of land
1099 surface water and energy fluxes for general circulation models. *Journal of Geophysical Research:*
1100 *Atmospheres*, 99(D7), 14415-14428.
- 1101 Liang, X., Wood, E. F., & Lettenmaier, D. P. (1996). Surface soil moisture parameterization of the VIC-2L model:
1102 Evaluation and modification. *Global and Planetary Change*, 13(1-4), 195-206.
- 1103 Liang, X., & Xie, Z. (2001). A new surface runoff parameterization with subgrid-scale soil heterogeneity for land
1104 surface models. *Advances in Water Resources*, 24(9-10), 1173-1193.
- 1105 Liang, X., & Xie, Z. (2003). Important factors in land–atmosphere interactions: surface runoff generations and
1106 interactions between surface and groundwater. *Global and Planetary Change*, 38(1-2), 101-114.
- 1107 Liang, X., Xie, Z., & Huang, M. (2003). A new parameterization for surface and groundwater interactions and its
1108 impact on water budgets with the variable infiltration capacity (VIC) land surface model. *Journal of
1109 Geophysical Research: Atmospheres*, 108(D16).
- 1110 Lu, Y., Duursma, R. A., & Medlyn, B. E. (2016). Optimal stomatal behaviour under stochastic rainfall. *Journal of
1111 theoretical biology*, 394, 160-171.
- 1112 Luo, X., Liang, X., & Lin, J. S. (2016). Plant transpiration and groundwater dynamics in water-limited climates:
1113 Impacts of hydraulic redistribution. *Water Resources Research*, 52(6), 4416-4437.
- 1114 Luo, X., Liang, X., & McCarthy, H. R. (2013). VIC+ for water-limited conditions: A study of biological and
1115 hydrological processes and their interactions in soil-plant-atmosphere continuum. *Water Resources
1116 Research*, 49(11), 7711-7732.
- 1117 Manzoni, S., Vico, G., Palmroth, S., Porporato, A., & Katul, G. (2013). Optimization of stomatal conductance for
1118 maximum carbon gain under dynamic soil moisture. *Advances in Water Resources*, 62, 90-105.
- 1119 Medlyn, B. E., Duursma, R. A., Eamus, D., Ellsworth, D. S., Prentice, I. C., Barton, C. V., et al. (2011). Reconciling
1120 the optimal and empirical approaches to modelling stomatal conductance. *Global Change Biology*, 17(6),
1121 2134-2144.
- 1122 Miner, G. L., Bauerle, W. L., & Baldocchi, D. D. (2017). Estimating the sensitivity of stomatal conductance to
1123 photosynthesis: a review. *Plant, cell & environment*, 40(7), 1214-1238.

- 1124 MÄKELÄ, A., BERNINGER, F., & HARI, P. (1996). Optimal control of gas exchange during drought: theoretical
 1125 analysis. *Annals of Botany*, 77(5), 461-468.
- 1126 Nobel, P. (1999). Leaves and fluxes. *Physicochemical and environmental plant physiology*, 2, 293-349.
- 1127 Prentice, I. C., Dong, N., Gleason, S. M., Maire, V., & Wright, I. J. (2014). Balancing the costs of carbon gain and
 1128 water transport: testing a new theoretical framework for plant functional ecology. *Ecology letters*, 17(1),
 1129 82-91.
- 1130 Prentice, I. C., Liang, X., Medlyn, B. E., & Wang, Y.-P. (2015). Reliable, robust and realistic: the three R's of next-
 1131 generation land-surface modelling. *Atmospheric Chemistry and Physics*, 15(10), 5987-6005.
- 1132 Rogers, A., Kumarathunge, D. P., Lombardozzi, D. L., Medlyn, B. E., Serbin, S. P., & Walker, A. P. (2021). Triose
 1133 phosphate utilization limitation: an unnecessary complexity in terrestrial biosphere model representation of
 1134 photosynthesis. *New Phytologist*, 230(1), 17-22.
- 1135 Schulze, E.-D., & Hall, A. (1982). Stomatal responses, water loss and CO₂ assimilation rates of plants in
 1136 contrasting environments. In *Physiological plant ecology II* (pp. 181-230): Springer.
- 1137 Schymanski, S. J., Sivapalan, M., Roderick, M., Hutley, L. B., & Beringer, J. (2009). An optimality-based model of
 1138 the dynamic feedbacks between natural vegetation and the water balance. *Water Resources Research*,
 1139 45(1).
- 1140 Sperry, J. S., Venturas, M. D., Anderegg, W. R., Mencuccini, M., Mackay, D. S., Wang, Y., & Love, D. M. (2017).
 1141 Predicting stomatal responses to the environment from the optimization of photosynthetic gain and
 1142 hydraulic cost. *Plant, cell & environment*, 40(6), 816-830.
- 1143 Stocker, B. D., Wang, H., Smith, N. G., Harrison, S. P., Keenan, T. F., Sandoval, D., et al. (2020). P-model v1. 0: an
 1144 optimality-based light use efficiency model for simulating ecosystem gross primary production.
 1145 *Geoscientific Model Development*, 13(3), 1545-1581.
- 1146 Sun, R., Hernández, F., Liang, X., & Yuan, H. (2020). A Calibration Framework for High-Resolution Hydrological
 1147 Models Using a Multiresolution and Heterogeneous Strategy. *Water Resources Research*, 56(8),
 1148 e2019WR026541.
- 1149 Tardieu, F., & Davies, W. (1993). Integration of hydraulic and chemical signalling in the control of stomatal
 1150 conductance and water status of droughted plants. *Plant, Cell & Environment*, 16(4), 341-349.
- 1151 Tuzet, A., Perrier, A., & Leuning, R. (2003). A coupled model of stomatal conductance, photosynthesis and
 1152 transpiration. *Plant, Cell & Environment*, 26(7), 1097-1116.
- 1153 Urban, O., Klem, K., Holišová, P., Šigut, L., Šprtová, M., Teslová-Navrátilová, P., et al. (2014). Impact of elevated
 1154 CO₂ concentration on dynamics of leaf photosynthesis in *Fagus sylvatica* is modulated by sky conditions.
 1155 *Environmental Pollution*, 185, 271-280.
- 1156 Wang, Y., Sperry, J. S., Anderegg, W. R., Venturas, M. D., & Trugman, A. T. (2020). A theoretical and empirical
 1157 assessment of stomatal optimization modeling. *New Phytologist*, 227(2), 311-325.
- 1158 Westhoff, M. C., Zehe, E., & Schymanski, S. J. (2014). Importance of temporal variability for hydrological
 1159 predictions based on the maximum entropy production principle. *Geophysical Research Letters*, 41(1), 67-
 1160 73.
- 1161 Wigmosta, M. S., Nijssen, B., Storck, P., & Lettenmaier, D. (2002). The distributed hydrology soil vegetation
 1162 model. *Mathematical models of small watershed hydrology and applications*, 7-42.
- 1163 Wigmosta, M. S., Vail, L. W., & Lettenmaier, D. P. (1994). A distributed hydrology-vegetation model for complex
 1164 terrain. *Water resources research*, 30(6), 1665-1679.
- 1165 Wolf, A., Anderegg, W. R., & Pacala, S. W. (2016). Optimal stomatal behavior with competition for water and risk
 1166 of hydraulic impairment. *Proceedings of the National Academy of Sciences*, 113(46), E7222-E7230.
- 1167 Zhou, S., Duursma, R. A., Medlyn, B. E., Kelly, J. W., & Prentice, I. C. (2013). How should we model plant
 1168 responses to drought? An analysis of stomatal and non-stomatal responses to water stress. *Agricultural and
 1169 Forest Meteorology*, 182, 204-214.

1171

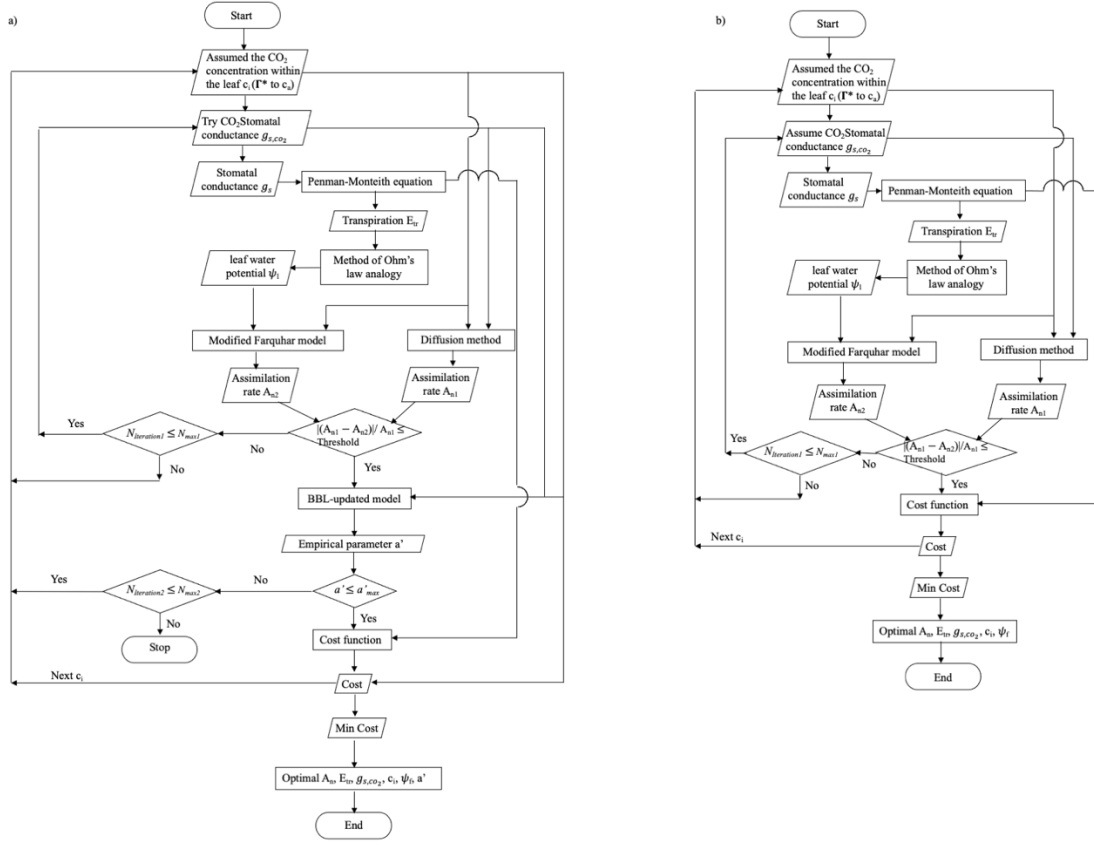


Figure 1. Flowchart of (a) The New approach, and (b) LC-extended approach.

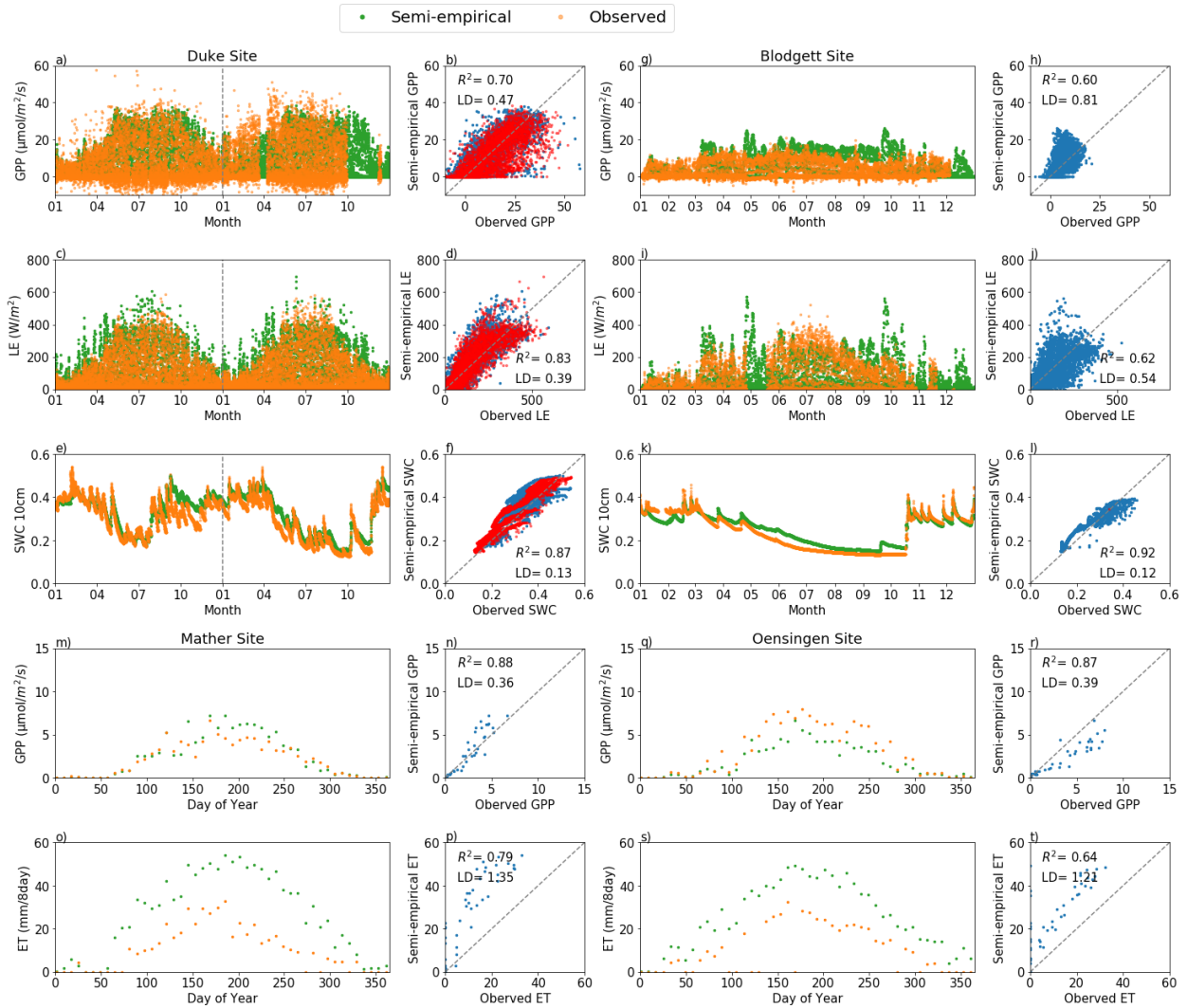


Figure 2. Comparison of the results using calibrated parameters by the Semi-empirical approach (green dots) with observations (orange dots). Plots (a)-(f): Hourly results over two years at the Duke site. Plots (g)-(l): Hourly results over one year at the Blodgett site. (m)-(p): 8-day results over one year at the Mather site. (q)-(t): 8-day results over one year at the Oensingen Site. (a), (b), (g), and (h) represent gross primary productivity (GPP); (c), (d), (i), and (j) latent heat flux (LE); (e), (f), (k), and (l) soil water content (SWC) at the depth of 10 cm; (m), (n), (q), and (r) represent gross primary productivity (GPP); and (o), (p), (s), and (t) 8-day total evapotranspiration (ET). For the Duke site, results on the left side of the vertical black dotted line in (a), (c) and (e) are for the calibration period while results on the right side are for the validation period.

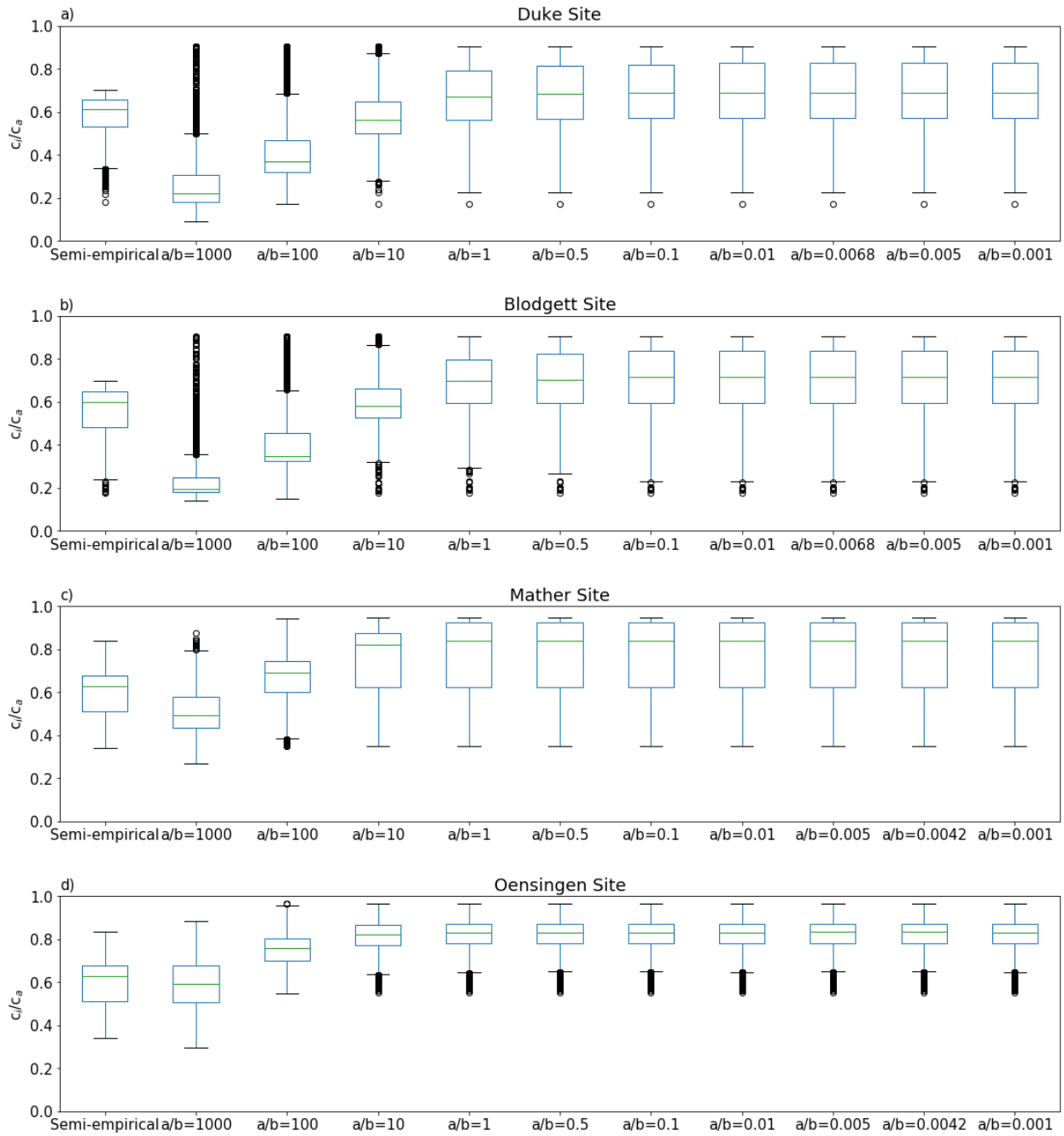


Figure 3. Sensitivity analysis between c_i/c_a and the different ratios of a/b in Eq. (7): (a) Duke site, (b) Blodgett site, (c) Mather site, and (d) Oensingen Site.

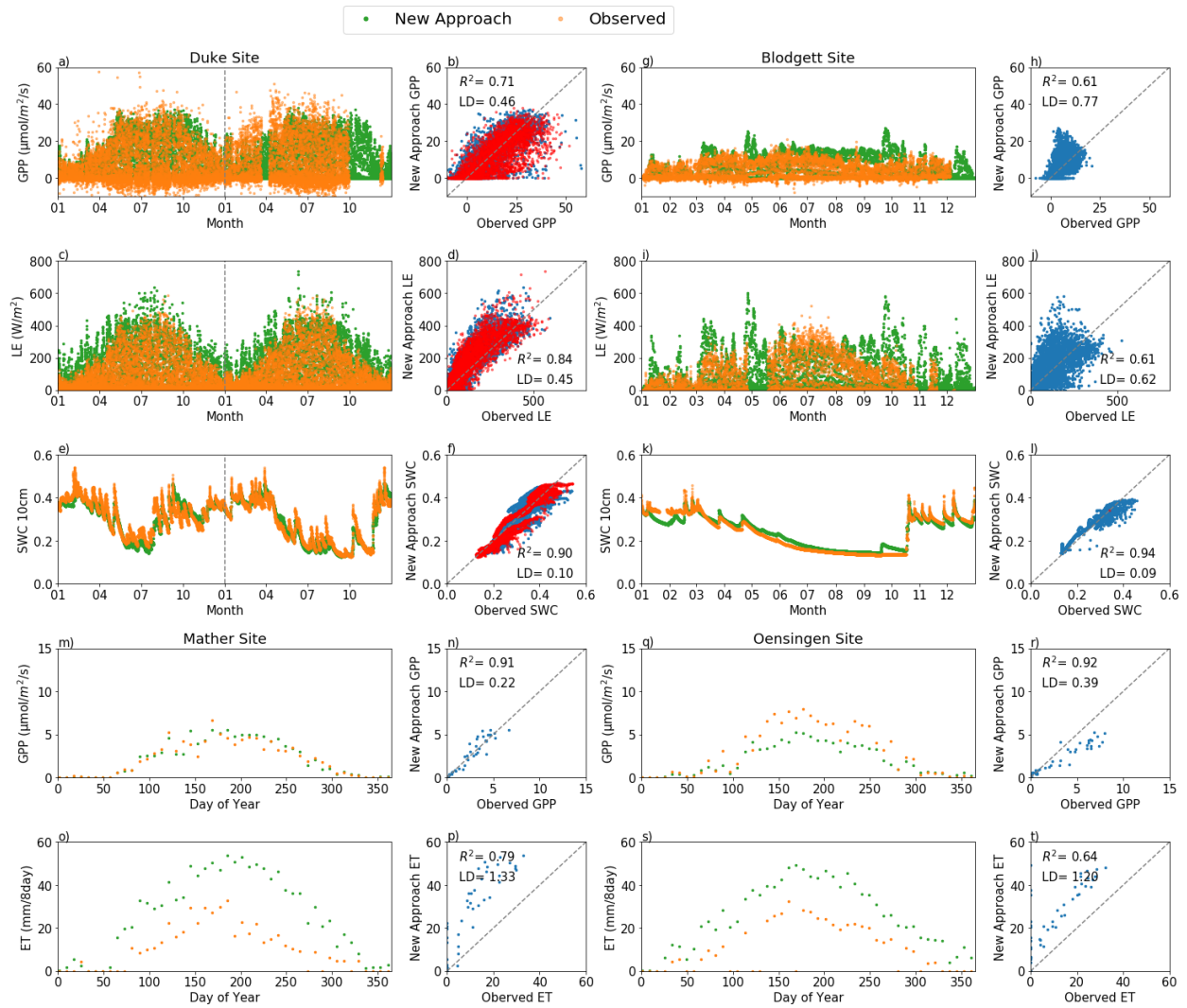


Figure 4. Comparison of the results using the same calibrated parameters by the New approach (green dots) with observations (orange dots). The notations used are the same as those in Fig. 2.

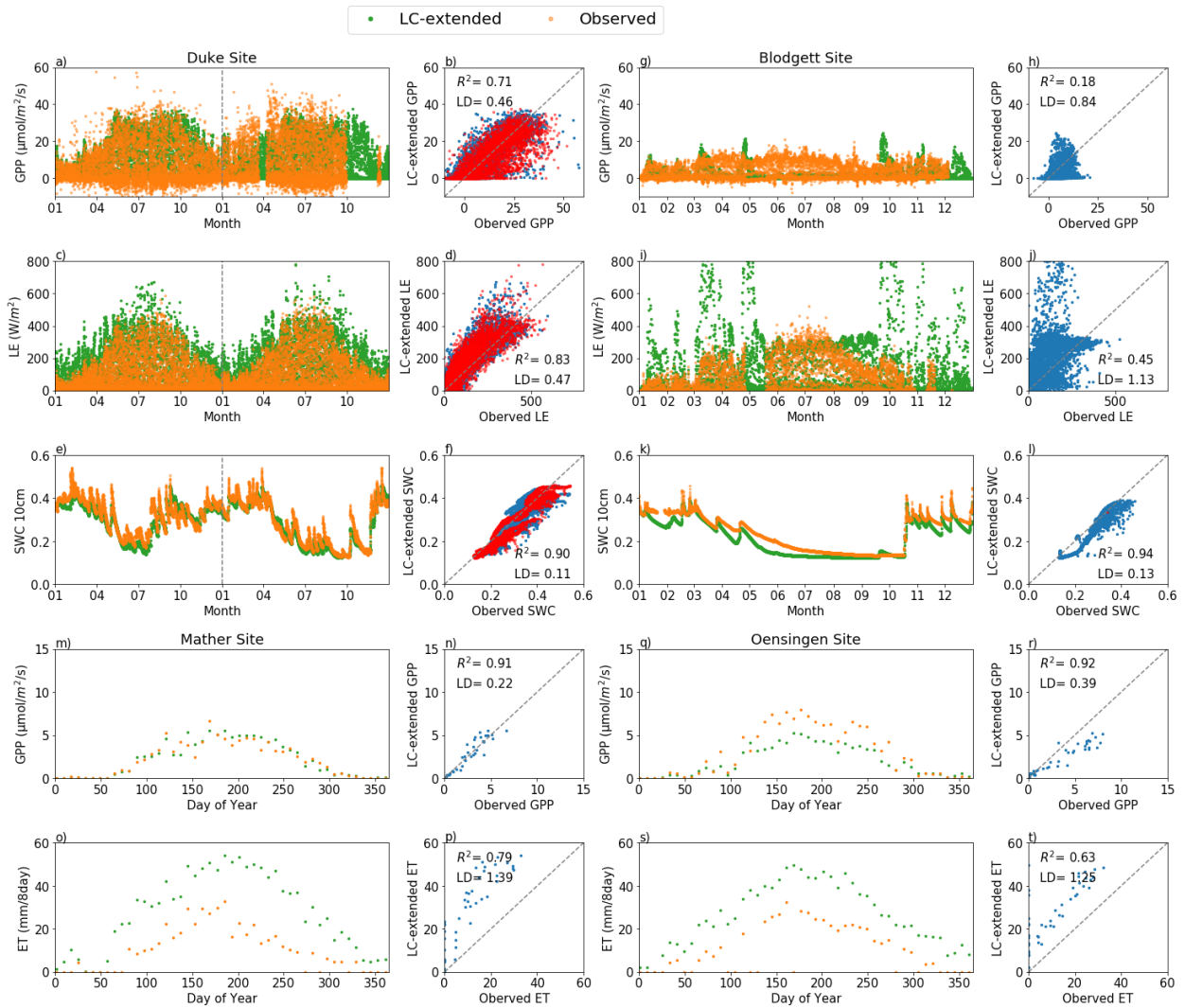


Figure 5. Comparison of the results using the same calibrated parameters by the LC-extended (green dots) with observations (orange dots). The notations used are the same as those in Fig. 2.

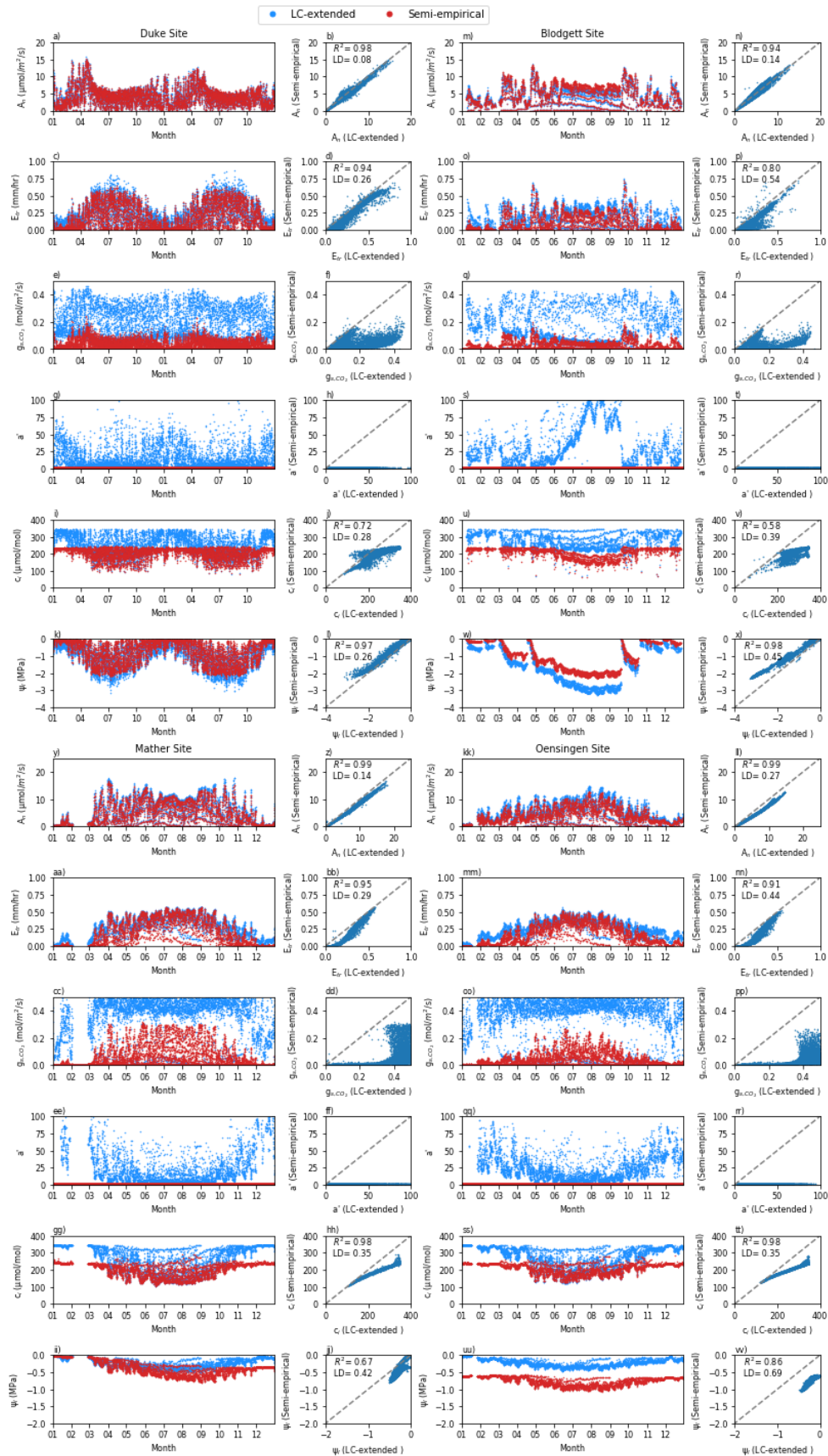


Figure 6. Comparison of results between the LC-extended approach (green dots) and Semi-empirical (red dots) over 8AM to sunset. (a)-(l): Hourly results over two years at Duke site; (m)-(x): Hourly results over one year at Blodgett site; (y)-(jj): Hourly results over one year at Mather site; (kk)-(vv): Hourly results over one year at Oensingen Site; (a), (b), (m), (n), (y), (z), (kk), and (ll) represent carbon assimilation (A_n); (c), (d), (o), (p), (aa), (bb), (mm), and (nn) plant transpiration (E_{tr}); (e), (f), (q), (r), (cc), (dd), (oo), and (pp) CO₂ stomatal conductance (g_{s,co_2}); (g), (h), (s), (t), (ee), (ff), (qq), and (rr) empirical coefficient (a'); (i), (j), (u), (v), (gg), (hh), (ss), and (tt) leaf CO₂ concentration (c_i); and (k), (l), (w), (x), (ii), (jj), (uu), and (vv) leaf water potential (ψ_l). The LD in the figure are calculated with a reference to the values from the semi-empirical approach.

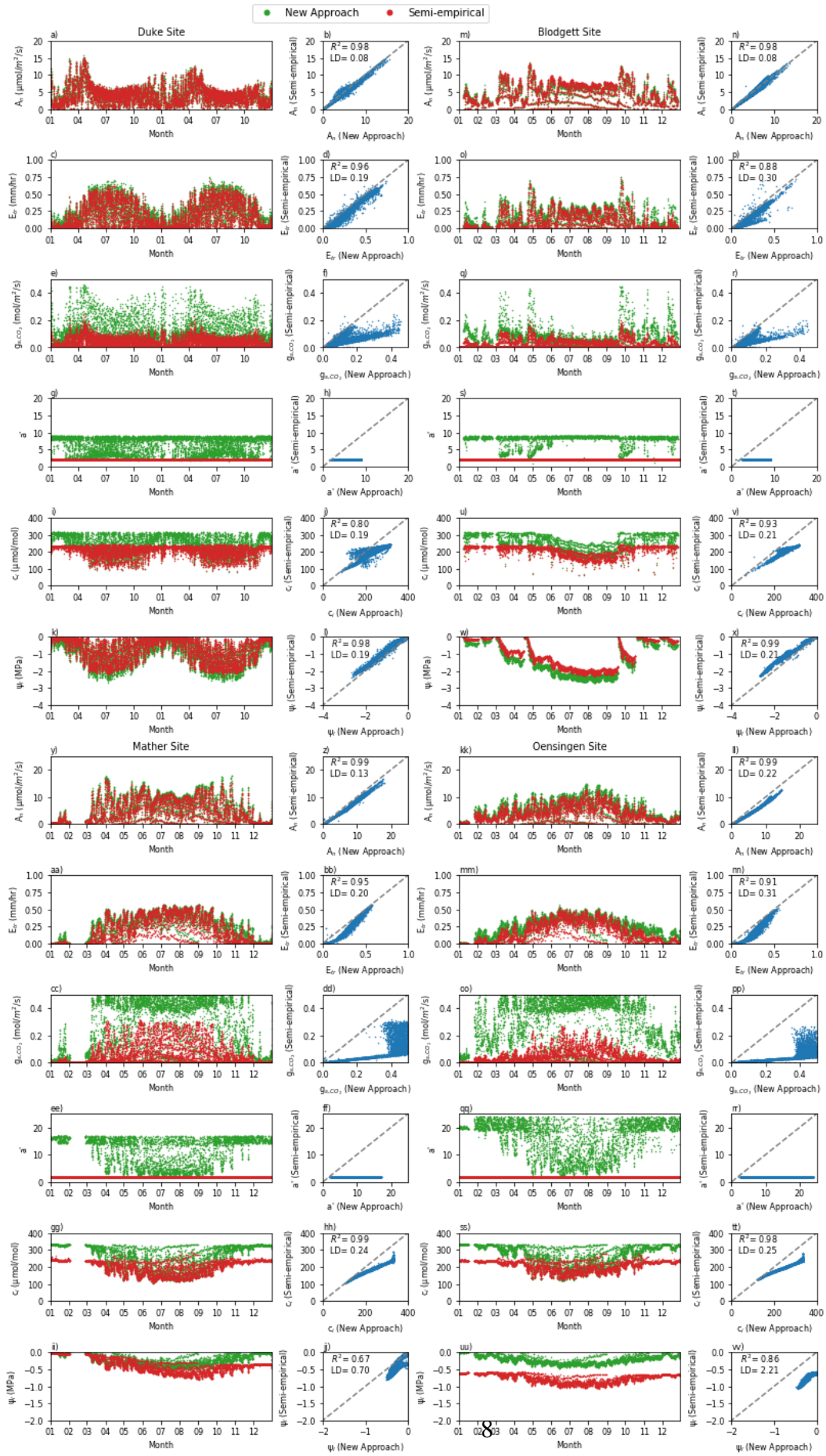


Figure 7. Comparison of the results between the New approach (green dots) and the Semi-empirical approach (red dots) over 8AM to sunset. (a)-(l): Hourly results over two years at Duke site; (m)-(x): Hourly results over one year at Blodgett site; (y)-(jj): Hourly results over one year at Mather site; (kk)-(vv): Hourly results over one year at Oensingen Site; (a), (b), (m), (n), (y), (z), (kk), and (ll) represent carbon assimilation (A_n); (c), (d), (o), (p), (aa), (bb), (mm), and (nn) plant transpiration (E_{tr}); (e), (f), (q), (r), (cc), (dd), (oo), and (pp) CO₂ stomatal conductance (g_{s,co_2}); (g), (h), (s), (t), (ee), (ff), (qq), and (rr) empirical coefficient (a'); (i), (j), (u), (v), (gg), (hh), (ss), and (tt) leaf CO₂ concentration (c_i); and (k), (l), (w), (x), (ii), (jj), (uu), and (vv) leaf water potential (ψ_l). The LD in the figure are calculated with a reference to the values from the New approach.

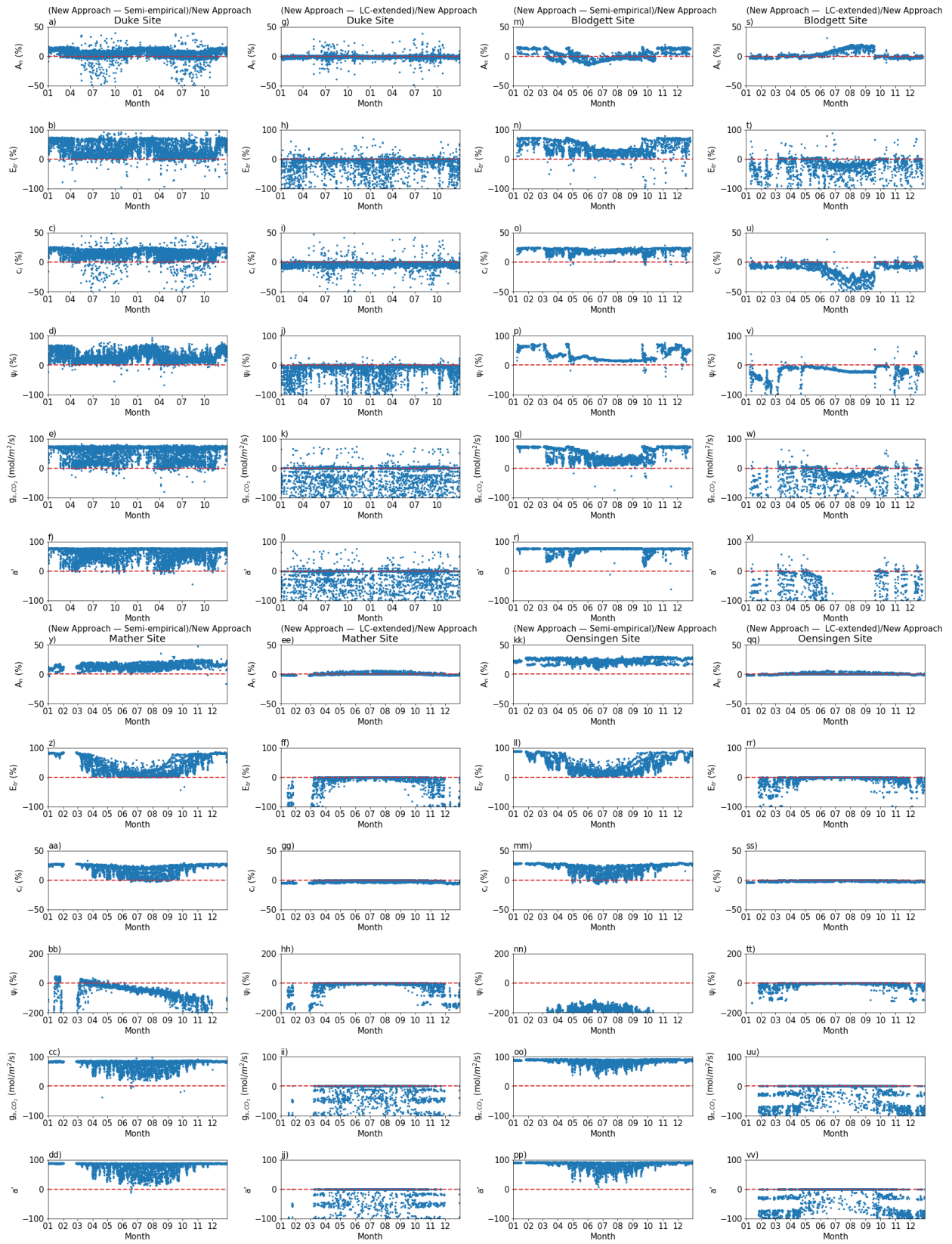


Figure 8. Relative differences between New approach and Semi-empirical and between New approach and LC-extended over 8AM to sunset. The first 4 rows are for the two forest sites with columns 1-2 for the Duke site and columns 3-4 the Blodgett site. The bottom 4 rows are for the two grassland sites with columns 1-2 for the Mather site and columns 3-4 the Oensingen site. Some of the relative differences between New Approach and LC-Extended are outside the plot bounds and not plotted. The percentages of data outside the plots displayed are as follows: (1) for the Duke site, they are 13.6%, 5.2%, 42.2%, and 30.9% for E_{tr} , ψ_l , g_{s,co_2} , a' respectively; (2) for the Blodgett site, they are 18.4%, 7.0%, 42.4%, and 61.1%; (3) for the Mather site, they are 15.9%, 9.3%, 34.5%, and 34.4% ; and (4) for the Oensingen site, they are 7.6%, 5.2%, 18.4%, and 18.2%. For the variable ψ_l , its relative differences between New Approach and Semi-empirical have 17.7% and 59.2% data outside plot bounds for Mather and Oensingen respectively.

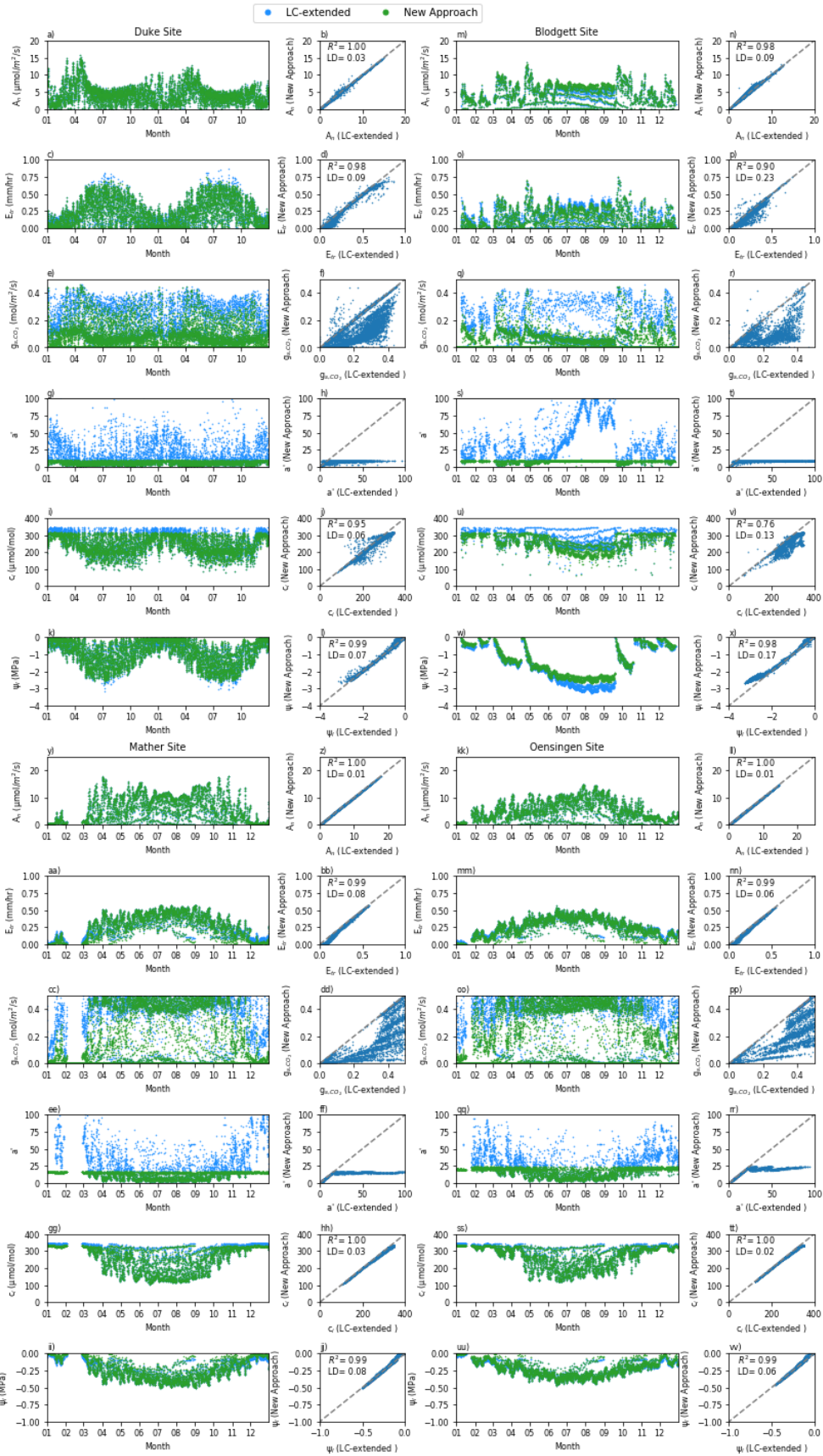


Figure 9. Comparison of results between the New approach (green dots) and the LC-extended approach (blue dots) over 8AM to sunset. Other notations are the same as those in Fig. 5. The LDs in the figure are calculated with a reference to the values from the New approach. Note that for a' , values greater than 100 from the Prentice-updated approach are not shown in the plots here. These large a' values account for, respectively, 1.9%, 1.1%, 9.3%, and 5.2%, for the Duke, Blodgett, Mather, and Oensingen sites.

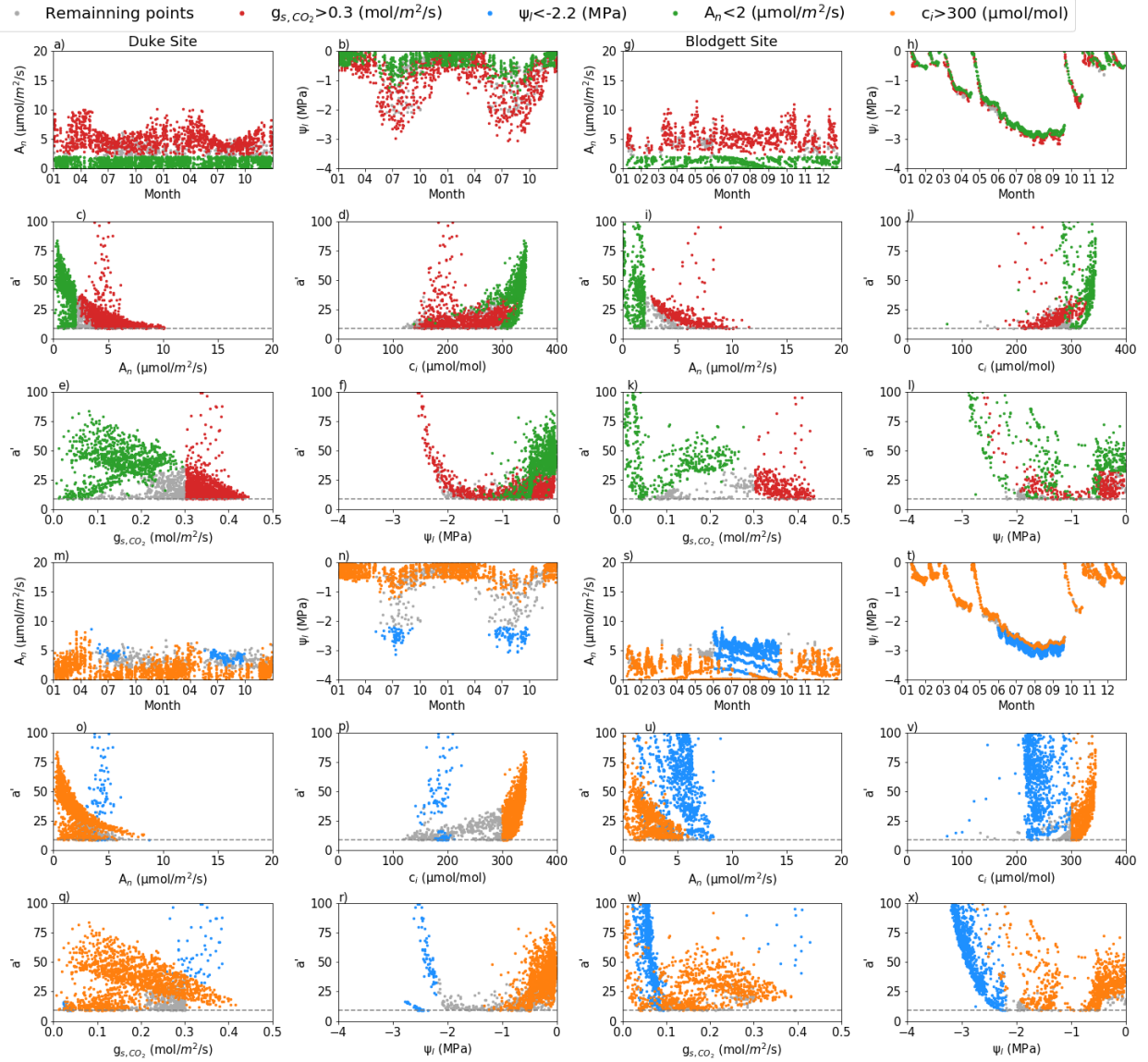


Figure 10a. Results over 8AM to sunset with the LC-extended approach at two sites in groups associated with $a' > a'_{max}$: $g_{s,co_2} > 0.3$ [mol/m²/s] (red dots), $\psi_l < -2.2$ [MPa] (blue dots), $A_n < 2$ [$\mu\text{mol}/\text{m}^2/\text{s}$] (green dots), $c_i > 300$ (orange dots), and data points not belonging to the preceding four groups (grey dots). (a)-(f) and (m)-(r): Duke site; (g)-(l) and (s)-(x): Blodgett site; (a), (g), (m), and (s) represent carbon assimilation (A_n); (b), (h), (n), and (t) leaf water potential (ψ_l); (c), (i), (o), and (u) empirical coefficient (a') vs. carbon assimilation (A_n); (d), (j), (p), and (v) empirical coefficient (a') vs. leaf CO₂ concentration (c_i); (e), (k), (q), and (w) empirical coefficient (a') vs CO₂ stomatal conductance (g_{s,co_2}); and (f), (l), (r) and (x) empirical coefficient (a') vs. leaf water potential (ψ_l). The dotted lines in each of the a' subplots represent their respective upper bound values. Like Figure 9, a' values greater than 100 are not shown in the plots here.

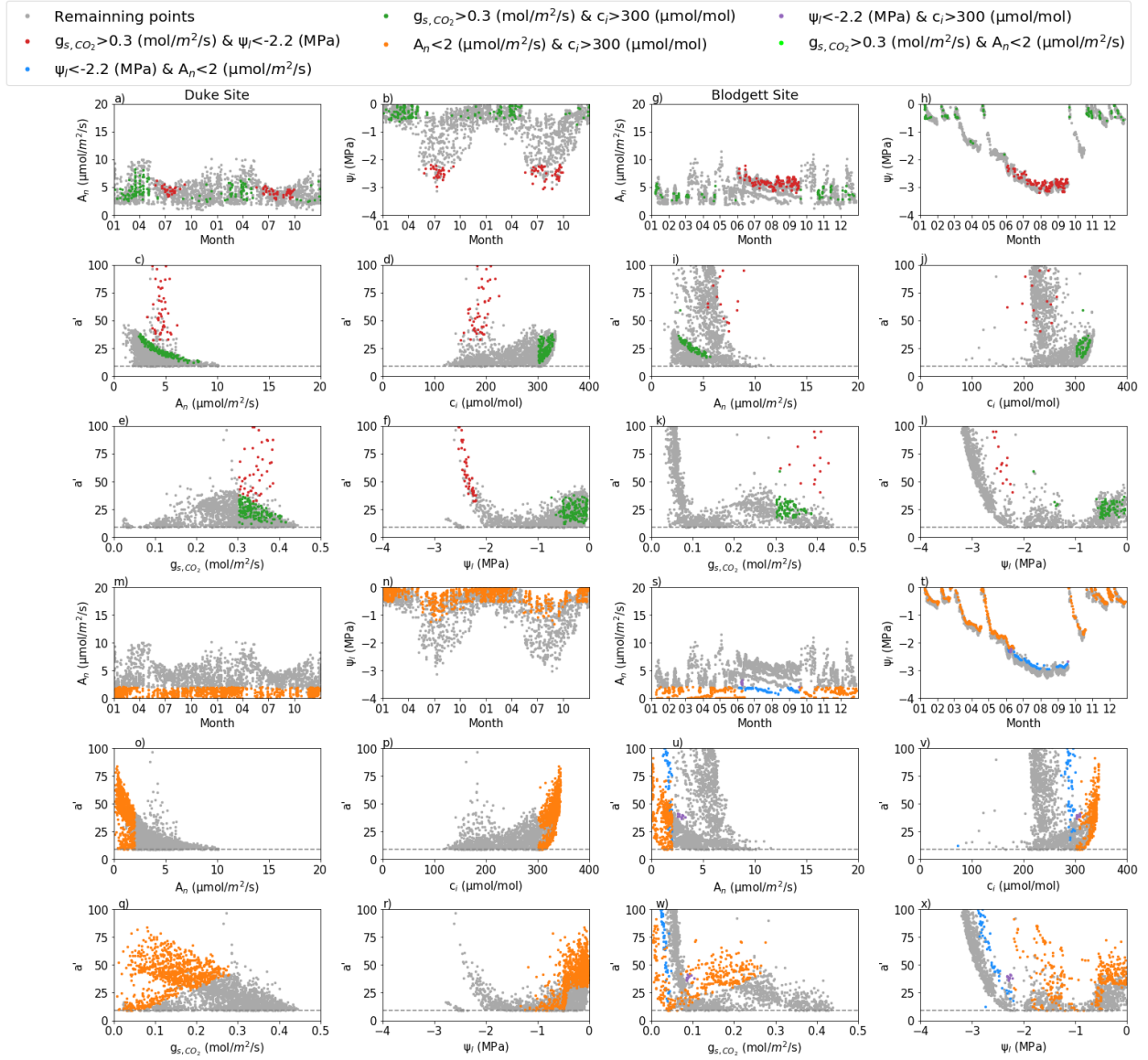


Figure 10b. The overlapping data points belonging to two groups shown in Figure 10a at the two forest sites by the LC-extended approach: overlapping between $\psi_l < -2.2$ [MPa] and $A_n < 2$ [$\mu\text{mol}/\text{m}^2/\text{s}$] (blue dots), between $A_n < 2$ [$\mu\text{mol}/\text{m}^2/\text{s}$] and $c_i > 300$ (orange dots), between $g_{s,\text{CO}_2} > 0.3$ [$\text{mol}/\text{m}^2/\text{s}$] and $\psi_l < -2.2$ [MPa] (red dots), between $g_{s,\text{CO}_2} > 0.3$ [$\text{mol}/\text{m}^2/\text{s}$] and $c_i > 300$ (green dots), between $\psi_l < -2.2$ [MPa] and $c_i > 300$ (purple dots), between $g_{s,\text{CO}_2} > 0.3$ [$\text{mol}/\text{m}^2/\text{s}$] and $A_n < 2$ [$\mu\text{mol}/\text{m}^2/\text{s}$] (lime dots), and remaining points (grey dots). These seven groups are not overlapping with each other. (c), (i), (o), and (u) empirical coefficient (a') vs. carbon assimilation (A_n); (d), (j), (p), and (v) empirical coefficient (a') vs. leaf CO_2 concentration (c_i); (e), (k), (q), and (w) empirical coefficient (a') vs CO_2 stomatal conductance (g_{s,CO_2}); and (f), (l), (r), (x) empirical coefficient (a') vs. leaf water potential (ψ_l). The dotted lines in each of the a' subplots represent their respective upper bound values (a'_{max}). Like Figure 9, a' values greater than 100 are not shown in the plots here.

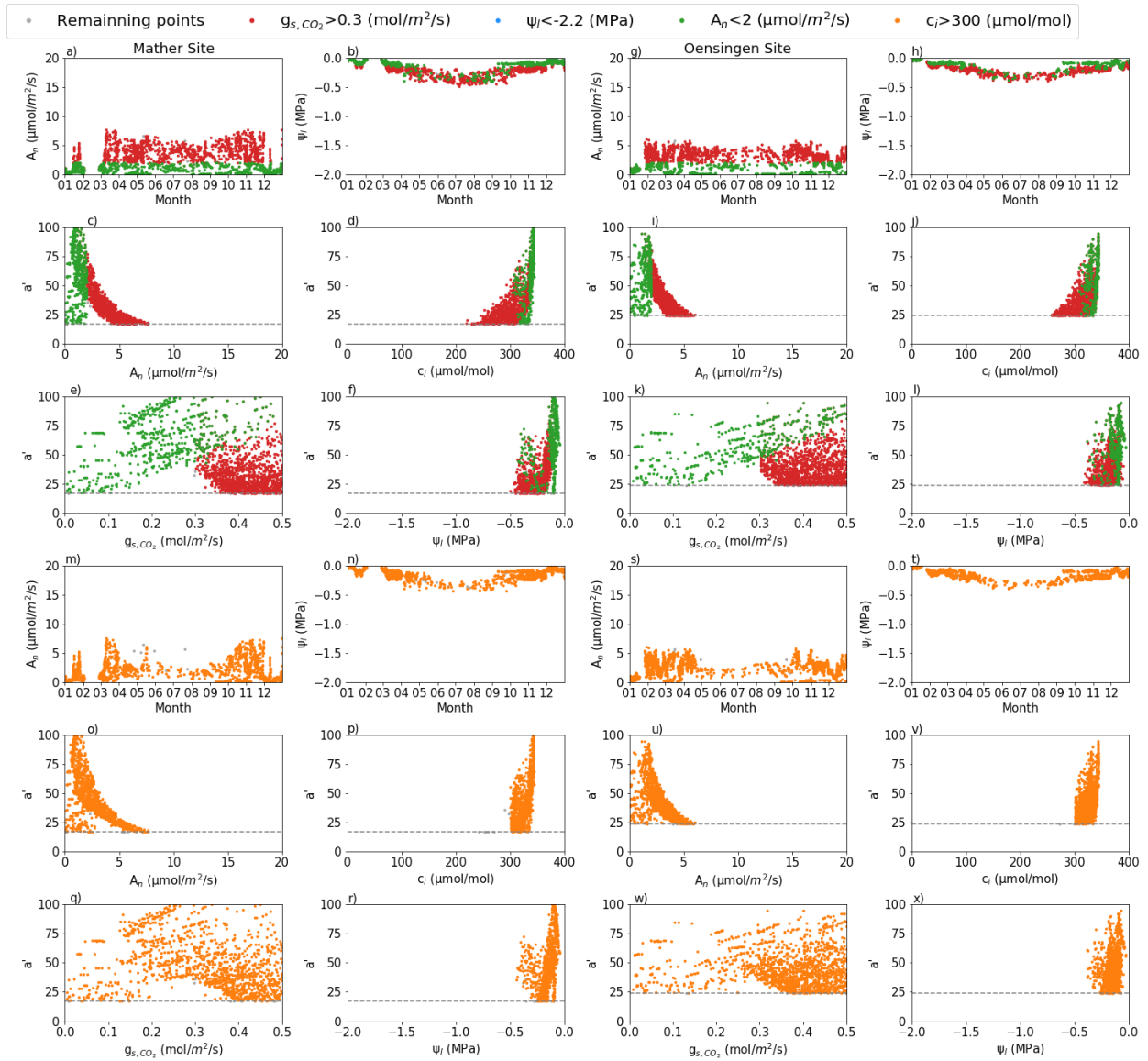


Figure 10c. Similar to Figure 10a, but for the Mather and Oensingen sites.

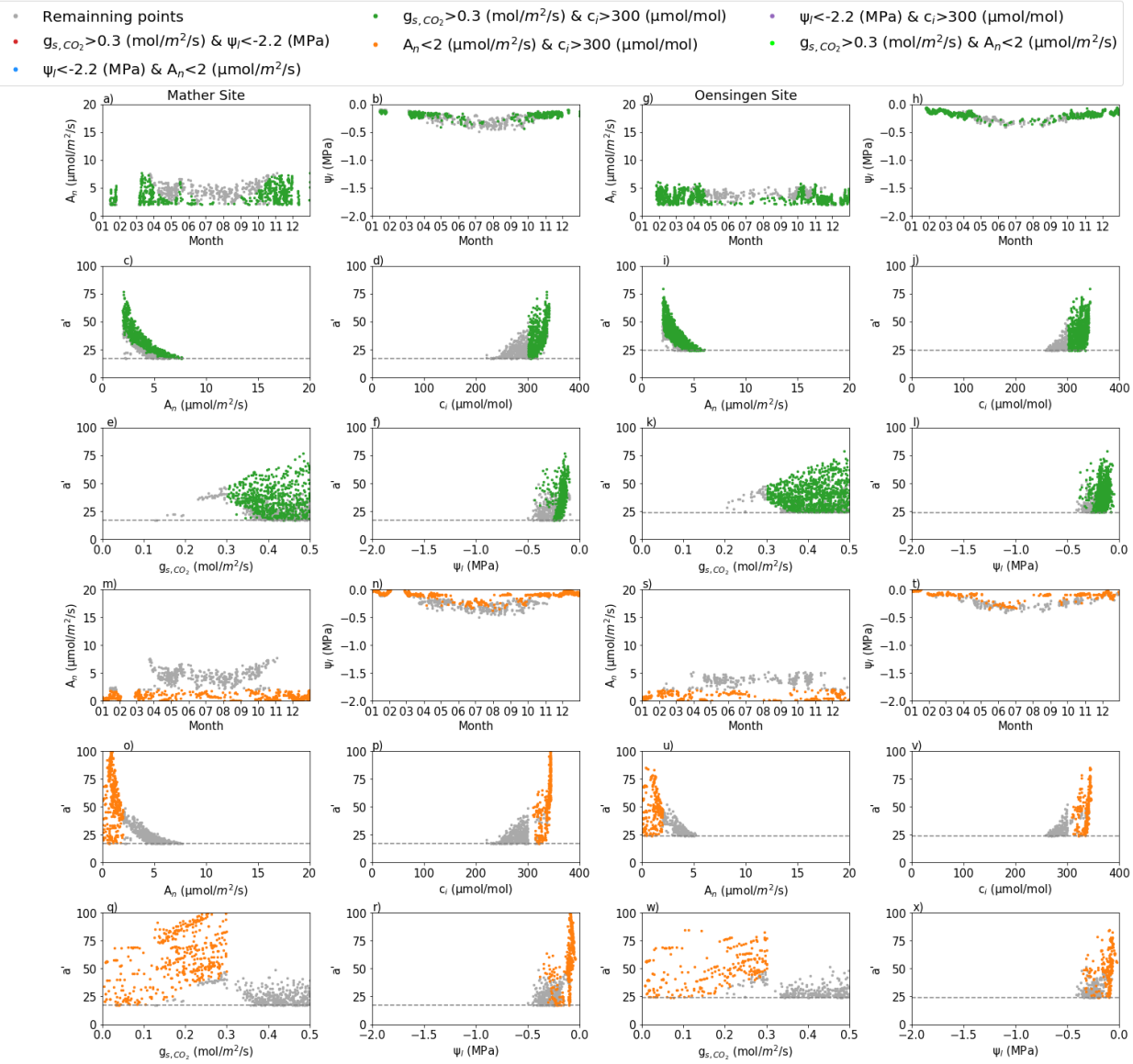


Figure 10d. Similar to Figure 10b, but for the Mather and Oensingen sites.

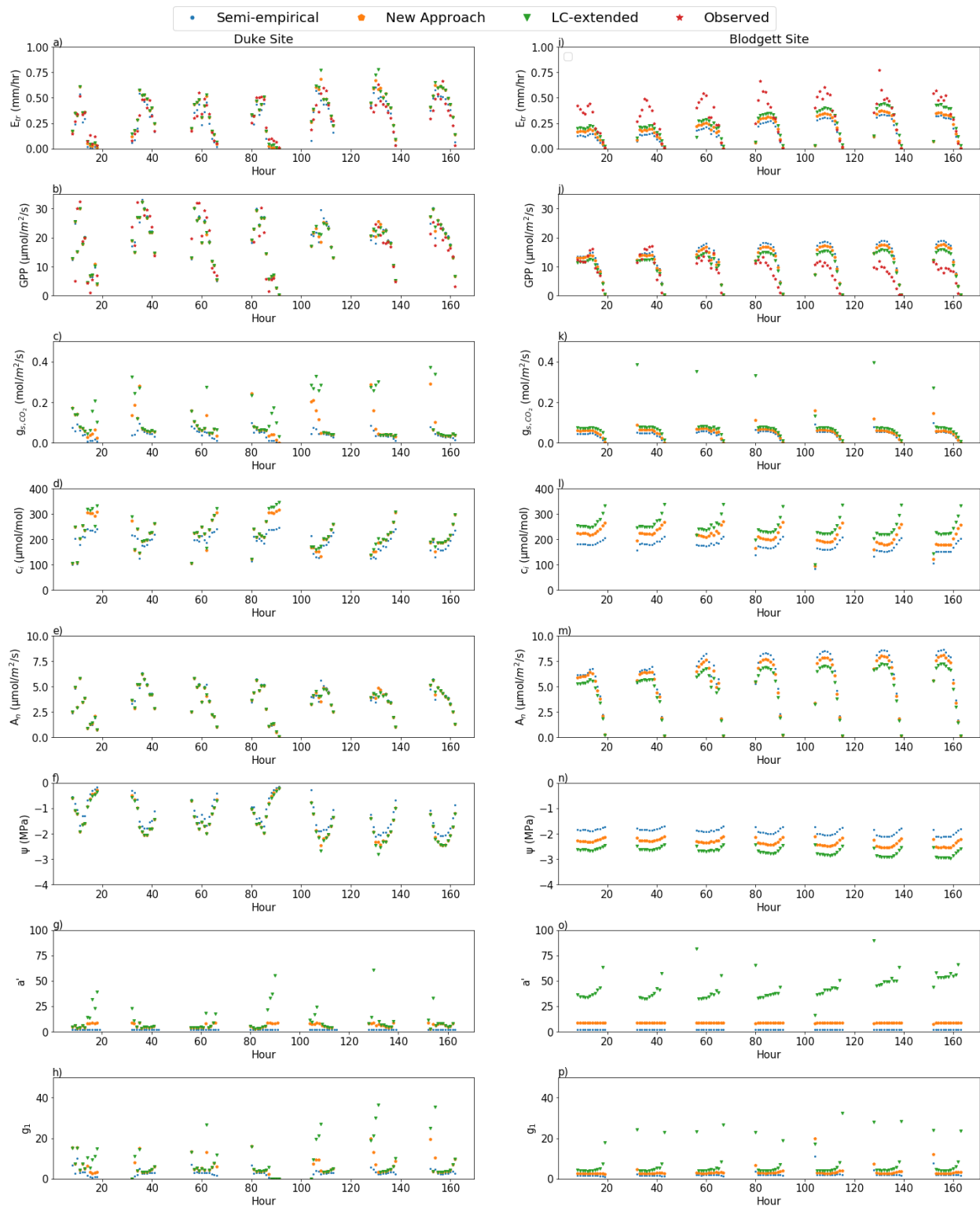


Figure 11. Comparison of one week hourly daytime results from June 30th to July 6th, 2004 among the New Approach, LC-extended, and the semi-empirical at the Duke site (a-h) and at the Blodgett site (i-p), respectively.

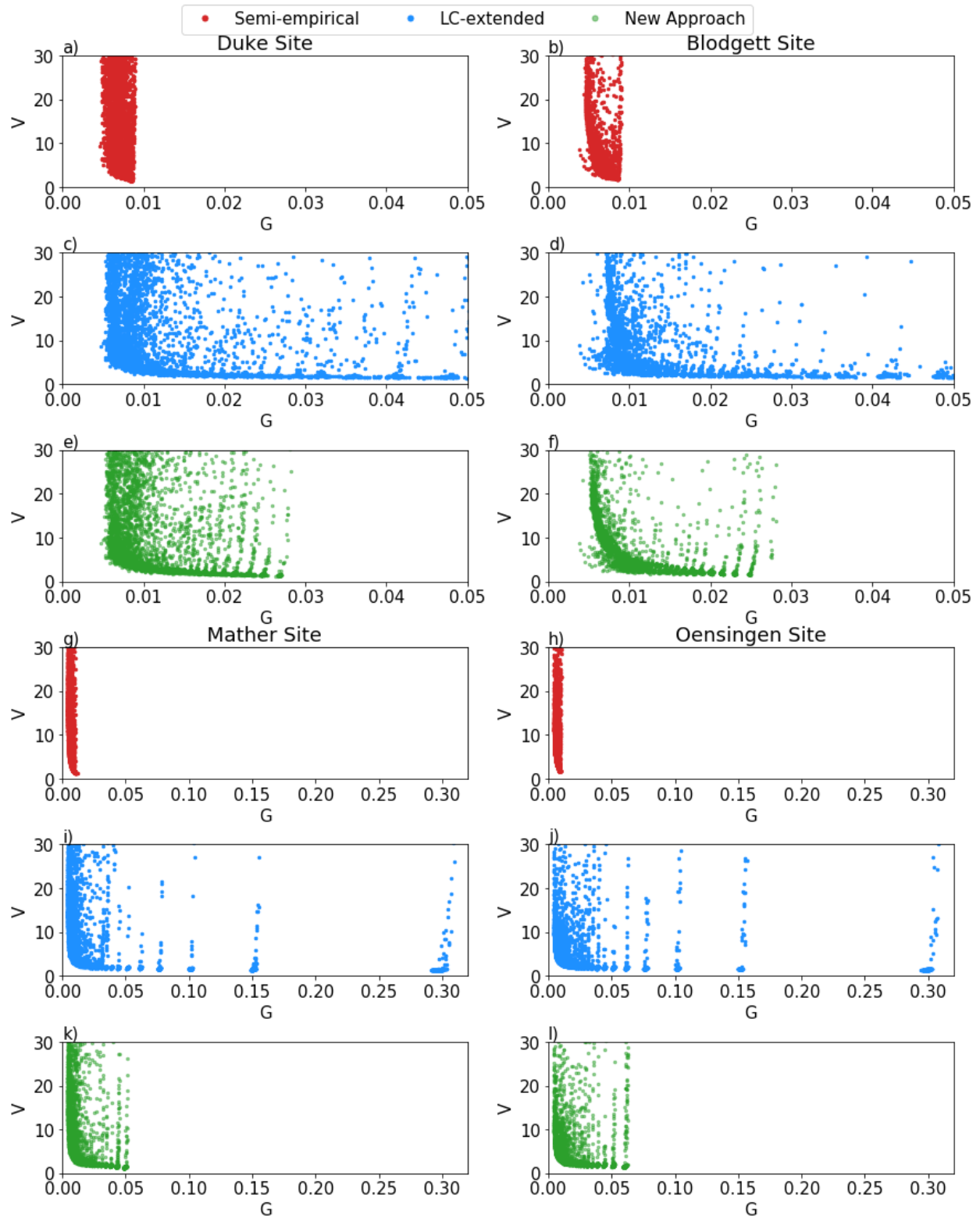


Figure 12. Comparison of the $V \sim G$ relationship among the Semi-empirical, LC-extended and New approach where $V = V_{cmax}/A_n$ and $G = g_{sab,co_2}/A_n$. (a), (c), and (e) are for the Duke site; (b), (d), and (f) the Blodgett site; (g), (i), and (k) the Mather site; (h), (j), (l) the Oensingen Site; (a), (b), (g), and (h) are from the Semi-empirical approach; (c), (d), (i), and (j) from the LC-extended approach; and (e), (f), (k), and (l) from the New approach.

Table 1. A list of model parameters calibrated for VIC+ and DHSVMm

VIC+		DHSVMm	
Parameters	Meaning	Parameters	Meaning
b	Exponent of variable infiltration capacity curve	K_{sat}	Lateral saturated hydraulic conductivity
W_s	Fraction of maximum soil moisture content of the lowest layer where nonlinear baseflow occurs	f	Exponent for change of lateral conductivity with depth (exponential decrease)
D_{smax}	Maximum velocity of baseflow	R_{omin}	Minimum stomatal resistance for the overstory
D_s	Fraction of D_{smax} where nonlinear baseflow begins	R_{umin}	Minimum stomatal resistance for the understory
d_2	The depth of 2 nd soil layer	f_c	Fraction coverage of overstory
d_3	The depth of 3 rd soil layer	μ	Aerodynamic attenuation
K_{rr}	Radial hydraulic conductivity of roots per unit of root surface area	θ_o	Soil moisture threshold to restrict transpiration for the overstory
K_{ra}	Axial hydraulic conductivity of roots per unit area	θ_u	Soil moisture threshold to restrict transpiration for the understory
Common parameters to both VIC+ and DHSVMm			
R_o	Reference resistance		
C	Capacity of plant water storage		
a'	An empirical coefficient (i.e., the slope) in BBL-updated equation		

Table 2. Investigation on reasonableness of variable values: 2a-2g from *LC-extended*, 2h from *New Approach* (Only daytime, 8AM to sunset, results are included.)

2a. Percentage of results that has $a' > a'_{\max}$

Duke Site	Blodgett Site	Mather Site	Oensigen Site
45.7	79.1	49.4	44.9

2b. Percentage of results in 2a satisfying four separations but overlapped groups

Site	$g_{s,co_2} > 0.3$	$\psi_l < -2.2$	$A_n < 2$	$c_i > 300$
Duke	33.3	4.8	36.0	53.6
Blodgett	16.5	46.7	22.8	42.7
Mather Site	60.1	0	47.5	81.1
Oensingen	74.5	0	33.6	86.9

Units: g_{s,co_2} in mol/m²/s; ψ_l in MPa, A_n in $\mu\text{mol}/\text{m}^2/\text{s}$, and c_i in $\mu\text{mol}/\text{mol}$.

2c. Percentage of results in 2a that fall into non-overlapping 2-groups

Site	$g_{s,co_2} > 0.3$ $\psi_l < -2.2$	$g_{s,co_2} > 0.3$ $A_n < 2$	$g_{s,co_2} > 0.3$ $c_i > 300$	$\psi_l < -2.2$ $A_n < 2$	$\psi_l < -2.2$ $c_i > 300$	$A_n < 2$ $c_i > 300^*$
Duke	2.3%	0%	5.1%	0%	0%	32.9%
Blodgett	4.0%	0%	3.4%	2.6%	0.9%	14.7%
Mather	0%	0%	32.6%	0%	0%	35.2%
Oensingen	0%	0%	52.4%	0%	0%	20.8%

*Note: percentages in this column exclude potentially reasonable results between 8AM and sunset.

2d. Percentage of results from 2a that belong to 3-groups

Site	$g_{s,co_2} > 0.3, \psi_l < -2.2,$ $A_n < 2$	$g_{s,co_2} > 0.3, \psi_l < -2.2,$ $c_i > 300$	$g_{s,co_2} > 0.3, A_n < 2,$ $c_i > 300$	$\psi_l < -2.2, A_n < 2,$ $c_i > 300$
Duke	0	0	0.3	0
Blodgett	0	0.1	0	5.0
Mather	0	0	9.8	0
Oensingen	0	0	10.4	0

Note: There is no result that simultaneously satisfies 4 grouping criteria.

2e. Percentage of results in 2a that belong to only one group and not to any other three groups listed in 2e

Site	$g_{s,co_2} > 0.3$ only	$\psi_l < -2.2$ only	$A_n < 2$ only	$c_i > 300$ only
Duke	25.9	2.5	2.4	15.1
Blodgett	9.3	34.6	0.5	19.3
Mather	18.9	0	0	2.1
Oensingen	13.1	0	0	2.3

2f. Percentage of results after further grouping of each single group from 2e

Site	$g_{s,co_2} > 0.3$ only		$\psi_l < -2.2$ only	$A_n < 2$ only	$c_i > 300$ only
	$ci < 200$ $Etr \geq 0.1$	$Etr < 0.1$ $200 < ci \leq 300$	$200 < ci \leq 300$ $g_{s,co_2} \leq 0.1$	$200 < ci \leq 300$	$5 \geq An \geq 2$ $0.1 < gs \leq 0.3$
Duke	30.6	22.1	5.1	94.6	94.5
Blodgett	0.4	42.5	99.0	100	91.6
	$200 < ci \leq 300$ $5 \geq An \geq 2, Etr > 0.2$				$0.2 < gs \leq 0.3$ $3 \geq An \geq 2$
Mather	64.2				83.3
Oensingen	93.5				97.7

Units: Etr in mm/hr

2g. Percentage of results in 2a that are deemed unreasonable

Site	*Unreasonable
Duke	*70.9
Blodgett	87.1
Mather	91.5
Oensingen	98.1

*= Sum of each cells in the row of Table 2c + sum of each cell of each row of Table 2d + (each cell of Table 2e) multiplied by (its corresponding unreasonable values occurrence in Table 2f)

For example, the percentage of unreasonable at the Duke site is:

$$* = (2.3\% + 5.1\% + 32.9\%) + 0.3\% + 25.9\% \times (30.6\% + 22.1\%) + 2.5\% \times 5.1\% + 2.4\% \times 94.6\% + 15.1\% \times 94.5\% = 70.9\%$$

2h. Percentage of *New Approach* results that are deemed unreasonable which all have $a' \leq a'_{max}$

Site	Unreasonable
Duke	9.3
Blodgett	3.2
Mather	3.9
Oensingen	6.2

Table 3. Percentage of $0 < G \leq 0.05$ and $0 < V \leq 30$ obtained from each approach

Site	Approach	$0 < G \leq 0.05$ [mol· μ mol ⁻¹]	$0 < V \leq 30$ [mol·mol ⁻¹]
Duke	New Approach	100	69
	LC-extended	91	69
	Semi-empirical	100	69
Blodgett	New Approach	100	90
	LC-extended	89	89
	Semi-empirical	100	90
Mather	New Approach	98	95
	LC-extended	75	95
	Semi-empirical	100	92
Oensingen	New Approach	86	98
	LC-extended	79	98
	Semi-empirical	100	97